



Hidden but Ubiquitous: The Pre-Rift Continental Mantle in the Red Sea Region

Alessio Sanfilippo^{1,2}, Camilla Sani¹, Najeeb M. A. Rasul³, Ian C. F. Stewart⁴, Luigi Vigliotti⁵, Nawaf Widinly³, Ahmed Osemi³ and Marco Ligi^{5*}

¹Dipartimento di Scienze della Terra e dell'Ambiente, Università di Pavia, Pavia, Italy, ²Istituto di Geoscienze e Georisorse – CNR, Pavia, Italy, ³Center for Marine Geology, Saudi Geological Survey, Jeddah, Saudi Arabia, ⁴Stewart Geophysical Consultants Pty. Ltd., College Park, SA, Australia, ⁵Istituto di Scienze Marine – CNR, Bologna, Italy

OPEN ACCESS

Edited by:

Froukje Marieke Van Der Zwan,
King Abdullah University of Science
and Technology, Saudi Arabia

Reviewed by:

Gilles Chazot,
Université de Bretagne Occidentale,
France
Tarun C. Khanna,
National Geophysical Research
Institute (CSIR), India

*Correspondence:

Marco Ligi
marco.ligi@bo.ismar.cnr.it

Specialty section:

This article was submitted to
Geochemistry,
a section of the journal
Frontiers in Earth Science

Received: 23 April 2021

Accepted: 22 July 2021

Published: 02 August 2021

Citation:

Sanfilippo A, Sani C, Rasul NMA,
Stewart ICF, Vigliotti L, Widinly N,
Osemi A and Ligi M (2021) Hidden but
Ubiquitous: The Pre-Rift Continental
Mantle in the Red Sea Region.
Front. Earth Sci. 9:699460.
doi: 10.3389/feart.2021.699460

Volcanism in the western part of the Arabian plate resulted in one of the largest alkali basalt provinces in the world, where lava fields with sub-alkaline to alkaline affinity are scattered from Syria and the Dead Sea Transform Zone through western Saudi Arabia to Yemen. After the Afar plume emplacement (~30 Ma), volcanism took place in Yemen and progressively propagated northward due to Red Sea rifting-related lithospheric thinning (initiated ~27–25 Ma). Few lava fields were emplaced during the Mesozoic, with the oldest 200 Ma volcanic activity recorded in northern Israel. We report results from volcanic pipes in the Marthoum area, east of Harrat Uwayrid, where over a hundred pipes occupy a stratigraphic level in the early Ordovician Saq sandstones. Most of them are circular or elliptical features marked by craters aligned along NW-SE fractures in the sandstone resulting from phreatomagmatic explosions that occurred when rising magma columns came in contact with the water table in the porous sandstone host. These lavas have Sr-Pb-Nd-Hf isotopic compositions far from the Cenozoic Arabian alkaline volcanism field, being considerably more enriched in Nd-Hf and Pb isotopes than any other Arabian Plate lava ever reported. New K-Ar dating constrains their age from Late Cretaceous to Early Eocene, thus anticipating the Afar plume emplacement and the Red Sea rift. Basalt geochemistry indicates that these volcanic eruptions formed from low-degree partial melting of an enriched lithospheric mantle source triggered by local variations in the asthenosphere-lithosphere boundary. This mantle source has a composition similar to the HIMU-like enriched isotopic component reported in the East African Rift and considered to represent the lowermost lithospheric mantle of the Nubian Shield. The generated melt, mixed in different proportions with melt derived from a depleted asthenosphere, produces the HIMU-like character throughout the Cenozoic Arabian alkaline volcanism. Although apparently hidden, this enriched lithospheric component is therefore ubiquitous and widespread in the cratonic roots of the African and Arabian subcontinental mantle.

Keywords: continental flood basalts, subcontinental mantle, HIMU-like mantle composition, Red-Sea rift, Nd-Hf-Sr-Pb isotopes

INTRODUCTION

Geochemical and petrological evidence of mantle peridotites and their basaltic counterparts indicate that the Earth's mantle is heterogeneous and formed by chemically depleted peridotites interspersed with fertile and chemically enriched heterogeneities (e.g., Zindler and Hart, 1986; Salters and Dick, 2002). Oceanic and continental basalts are commonly produced by the melting of a small portion of this heterogeneous mantle within a melting region that most likely exceeds the inherent spatial heterogeneity wavelength of the source material (McKenzie, 1986). This causes the melts produced by different components of the mantle to mix in the shallow mantle or in the overlying crust during the upward migration process (Stracke, 2012; Lambart et al., 2019; Stracke et al., 2019). Therefore, the isotopic imprint of source heterogeneities is generally obscured since these different isotopic entities tend to be diluted by mixing with the primary melt (Tackley, 2015; Stracke, 2016). This process shifts the composition of the melt and, rarely, erupted magmas are representative of melts in equilibrium with the mantle source (Rudge et al., 2013). However, basalts exhibit locally high geochemical and isotopic variability over small distances and/or over short time intervals, such as in a single dredge haul, or along the flanks of a central volcano along mid-ocean ridges (e.g., Niu and Batiza, 1997; Gale et al., 2011; Gale et al., 2013), or between overlapped lava flows from a single subaerial vent (Hofmann and Farnetani, 2013; Harrison et al., 2017). Hence, these lavas may preserve the isotopic variability of the source region, that can be resolved once the isotopic compositions of the most extreme “mantle components” are known.

Cenozoic volcanism in the Arabian plate is one of the largest alkali volcanic province on Earth. Here, ~180,000 km² of basalts with subalkaline to alkaline affinity form large lava fields scattered from Israel, Syria, Saudi Arabia to Yemen (Coleman et al., 1983) (**Figure 1**). These lavas erupted initially in Yemen following the emplacement of the Afar plume (~30 Ma; Stern and Johnson, 2010) and then progressively propagated northwards due to continental lithosphere thinning as a consequence of Red Sea rifting that initiated ~27–25 Ma (Bohannon et al., 1989; Bosworth and Stockli, 2016). However, some lava fields formed in the Early Cretaceous with the oldest 200 Ma volcanic activity recorded in Israel (Atlit-1 and Haifa-1 drillholes; Khon et al., 1993). The mantle source composition of Arabian volcanism varies on a regional scale due to mixing enriched mantle components with an isotopically depleted asthenospheric mantle source (i.e., with high Nd-Hf and low Sr-Pb isotopic ratios, Schilling et al., 1992) feeding Red Sea oceanic basalts (Altherr et al., 1988; Altherr et al., 1990; Haase et al., 2000; Ligi et al., 2012; Ligi et al., 2015; Ligi et al., 2018). The origin and composition of the enriched components is still debated. Basalts with relatively high Sr and high Pb, and low-Nd and -Hf isotopic ratios reveal the influence of the Afar Plume in the large lava fields of Yemen, Ethiopia (Chazot and Bertrand, 1993; Baker et al., 1996; Stewart and Rogers, 1996), Djibouti (Vidal et al., 1991; Deniel et al., 1994) and southern Arabia (Bertrand et al.,

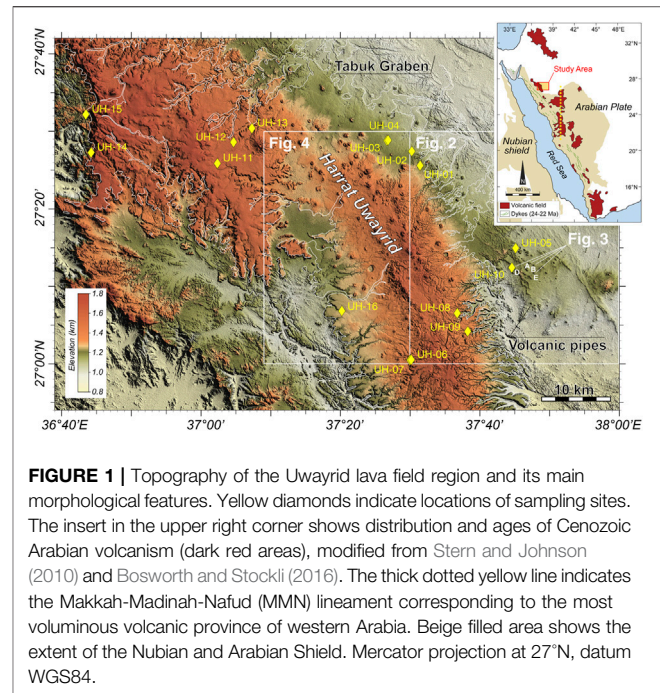


FIGURE 1 | Topography of the Uwayrid lava field region and its main morphological features. Yellow diamonds indicate locations of sampling sites. The insert in the upper right corner shows distribution and ages of Cenozoic Arabian volcanism (dark red areas), modified from Stern and Johnson (2010) and Bosworth and Stockli (2016). The thick dotted yellow line indicates the Makkah-Madinah-Nafud (MMN) lineament corresponding to the most voluminous volcanic province of western Arabia. Beige filled area shows the extent of the Nubian and Arabian Shield. Mercator projection at 27°N, datum WGS84.

2003). On the other hand, basalts from central and northern Arabia contain a distinct enriched mantle component with higher Pb and lower Sr ratios, and with Nd and Hf isotope contents similar to those of the Afar basalts (Bertrand et al., 2003; Shaw et al., 2003; Moufti et al., 2012; Altherr et al., 2019). The most extreme expression of this enriched component has been found in some lavas of the East African Rift (Rooney et al., 2014; Abu El-Rus et al., 2018), where their high Pb and extremely low Nd and Hf isotopic ratios point toward the “HIMU” (high $\mu = ^{238}\text{U}/^{204}\text{Pb}$) endmember, as defined for oceanic basalts (Zindler and Hart, 1986; Stracke et al., 2003). In the Nubian Plate, this component is thought to be located in the lithospheric mantle, and originated by an old metasomatic event that affected the north-eastern African lithospheric mantle during the Neoproterozoic Pan-African orogeny (Stein et al., 1997). However, the lack of such extreme compositions in Arabian magmatism casts doubt on the presence of this mantle enriched component at the roots of the Arabian subcontinental mantle.

Here, we report evidence of the presence in the lowermost lithospheric mantle of the Arabian plate of an enriched HIMU-like isotopic component, as sampled by volcanic pipes in northern Saudi Arabia (**Figure 1**) at the eastern boundary of the Arabian-Nubian Shield (ANS). Basaltic lavas from these pipes have Sr-Pb-Nd-Hf isotopic ratios similar to lavas of Gerba Guracha in the East African Rift (Rooney et al., 2014). Their compositions stand out from the alkaline field of the Cenozoic volcanism of Arabia, being far more enriched with low Nd-Hf and high Pb isotopes than any lava ever reported from the Arabian Plate. K-Ar dating constrains their age from the Late Cretaceous to the Early Eocene, thus predating the emplacement

of the Afar plume and of the Red Sea rift. These volcanic eruptions were formed by low degrees of partial melting of a chemically enriched mantle source, triggered by local depth variations of the asthenosphere-lithosphere boundary. This enriched lithospheric component, mixed in different proportions with melt derived from a depleted asthenosphere, provides the HIMU-like character present throughout the Cenozoic alkaline volcanism of Arabia, suggesting that although hidden, it is ubiquitous and widespread in the cratonic roots of the Arabian and African lithospheric mantle.

However, further sampling and geochemical analyses are required for a complete view and statistical robustness of the evidence reported in this work because results are from a limited set of samples from only two of the numerous volcanic pipes injected into the area.

GEOLOGICAL SETTING

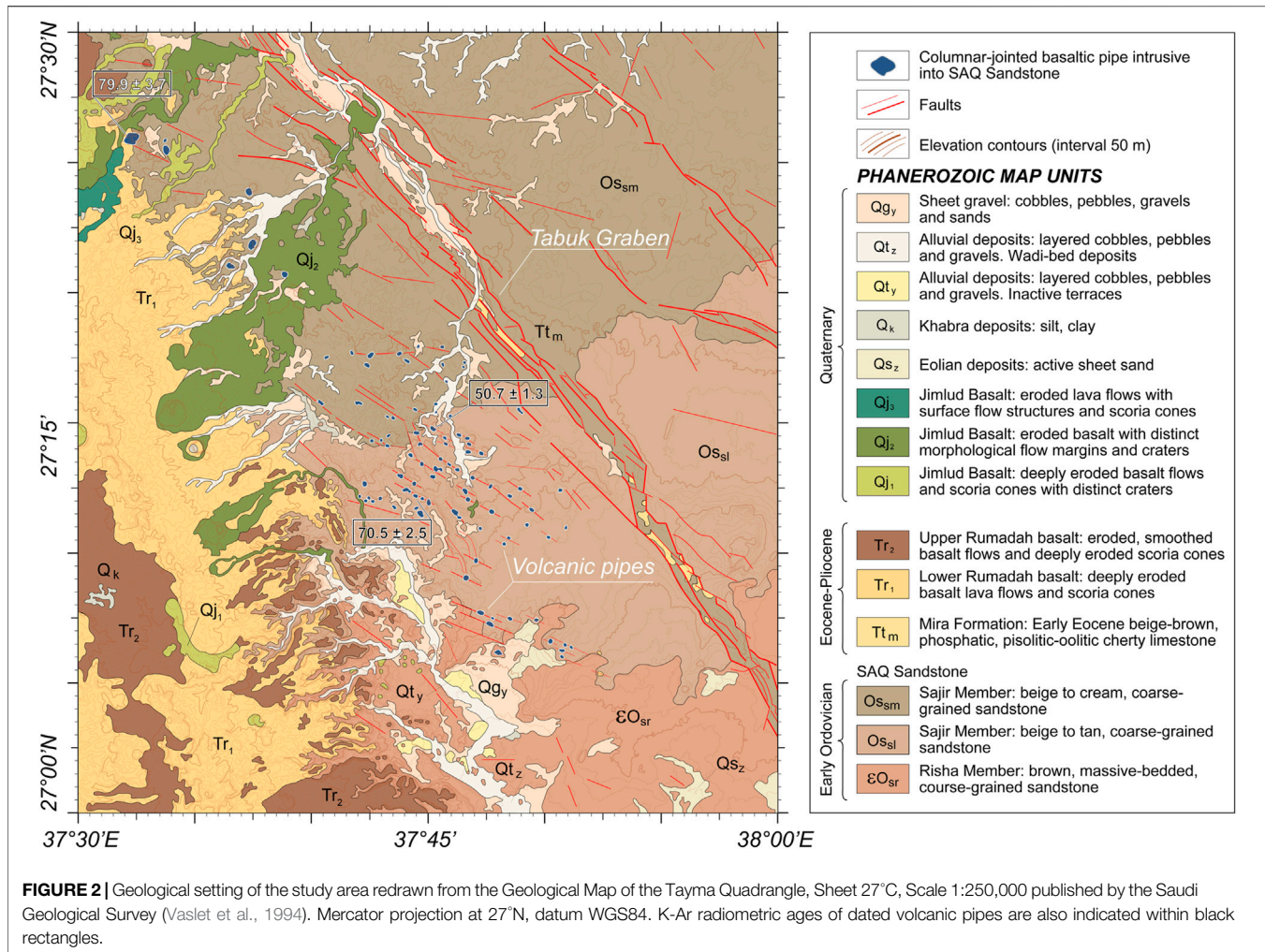
The Arabian Plate Cenozoic volcanism occurred from the Oligocene to the Quaternary, with the most intense magmatic cycle almost contemporaneous with the separation of Arabia from the African plate. Volcanism commenced after the emplacement of the Afar plume (30–35 Ma) with the formation of thick flood basalts widely diffused in the southern part of the Arabian Shield (Yemen Traps series; Volker et al., 1997; Bertrand et al., 2003), followed by the formation of large lava fields during the opening of the Red Sea (Baker et al., 1997; Rukieh et al., 2005). These lavas are mostly sodic alkali basalts, basanites, hawaiites and more rarely tholeiitic basalts (Barberi and Varet, 1977; Ibrahim et al., 2003; Shaw et al., 2003; Weinstein et al., 2006). Decompression mantle melting triggered by continental lithosphere extension and thinning (since 27–25 Ma) is considered the primary cause for magma genesis in the central and northern Arabian alkaline lava fields, called *harrat*. They span over a distance of 1,400 km in Syria, Israel and Saudi Arabia. Based on age determinations and structural trends, this Cenozoic alkaline volcanism is generally attributed to two distinct periods (Coleman et al., 1983; Camp and Roobol, 1992). The first period (30–15 Ma) was contemporaneous with thermal doming, stretching and thinning of the crystalline Precambrian basement of the Arabian–Nubian Shield along a NNW-SSE trending rift system in the Red Sea region (Camp and Roobol, 1992). In the early stages of rifting (24–22 Ma, Bosworth et al., 2005), several basaltic tholeiitic dikes were injected into the Arabian basement giving rise to a vast dike swarm running NNW-SSE parallel to the coast over the entire length of the Red Sea (Pallister, 1987; Coleman and McGuire, 1988). Furthermore, the magmatic activity generated voluminous basalt lava fields over the entire Arabian Peninsula with tholeiitic to transitional affinity including the Yemen Traps (30–26 Ma), and the As Sirat (30–25), Ash Shaam (27–22 Ma), Al Lith (26–22 Ma), Hadan (28–15 Ma) and Ishara (17–12 Ma) harrat. After a short period of inactivity, the recent volcanism (12 Ma-present) developed the Uwayrid and Al Buqum harrat (9 Ma - present), the N–S aligned volcanic fields of Rahat and Khaybar (11 Ma - present) along the so-called

Makkah-Madinah-Nafud (MMN) line (Figure 1), and the most recent, Al Kishb, Lunayyir, Al Birk and Hutaymah harrats (<2 Ma) (Camp and Roobol, 1992). During this period, volcanic products have evolved over time towards more alkaline compositions.

Volcanism in Arabia was almost absent during the Mesozoic and lower Tertiary; however, some Middle East lava fields predate the emplacement of the Afar plume. Alkaline volcanism developed in Israel since 200 Ma and continued until the Miocene (Lang and Steinitz, 1989), with the oldest volcanic activity being probably related to the emplacement of a Jurassic plume (Atlit-1 and Haifa-1 drill-holes, Khon et al., 1993). A Late Cretaceous volcanic field (~90 Ma) crops out in south-eastern Egypt (Natash volcanic province) at the same latitude of the Uwayrid lava field (Figure 1), where alkali-basalt lavas evolve locally towards trachytic and rhyolitic compositions (Abu el-Rus et al., 2018). The presence of lava fields with alkaline affinity during the Mesozoic suggests that the continental lithosphere of East Africa and Arabia was initially subject to diffuse extension with deformation by stretching and faulting (Rooney et al., 2011). In this scenario, scattered volcanic fields were triggered by melting of low-solidus metasomes at the lithosphere-asthenosphere boundary before continental necking and substantial crustal thinning (Ebinger et al., 1993; Mackenzie et al., 2005; White et al., 2008; Thybo and Nielsen, 2009; Rooney et al., 2011; Rooney et al., 2014).

Harrat Uwayrid

Samples were recovered from Harrat Uwayrid and from a subset of volcanic pipes outcropping along its eastern flank (Figures 1, 2). Harrat Uwayrid forms an elongated NW-SE lava field with areal extension of ~7,150 km², extending from north to south over ~230 km (Altherr et al., 2019). This volcanic field consists of a heavily eroded series of older plateau basalts, overlain by younger flows located mainly north of the Al Jaww depression (Brown et al., 1989; Coleman, 1993). Uwayrid's lavas are subdivided into two distinct stratigraphic units (Vaslet et al., 1994). The older Tertiary age unit (the Rumadah basalt) was produced by predominantly monogenetic volcanic activity with alignments of eruptive vents marked by scoria cones (Figure 2). There is also polygenetic eruptive activity, that includes large and more complex Strombolian scoria volcanoes. Tectonic uplift of the region followed the eruption of the Rumadah Formation, causing significant erosion and major erosive escarpments cut into the Rumadah basalt. The beginning of this tectonic activity marked the cessation of volcanic activity in correspondence with the Rumadah eruptive vents. The younger Quaternary volcanic formation, called the Jimlud basalt, was erupted from isolated and scattered cinder cones that lay on the oldest Rumadah lava flows without forming a continuous cover. Some notable maar craters and their associated collars of pyroclastic deposits are due to basaltic eruptions that encountered the near-surface water table (Figure 1). Basaltic magmas interacting with water produced phreatomagmatic explosions and the consequent



morphology. At the edge of the Rumadah Basaltic Plateau, the Jimlud lava flows have followed deep wadis incised in the older basalt; some of them emerged below the Rumadah lava's base and extended eastward over the eroded Saq sandstone beyond the limits of the plateau eroded margins (Figure 2). Based on K-Ar dating, Altherr et al. (2019) divided the volcanic activity of Harrat Uwayrid in three groups: Late Miocene, Pliocene and Quaternary volcanism. Miocene low-viscosity flows of the mildly alkaline Rumadah basalt were followed by Pliocene and Quaternary lavas ranging from basanites/tephrites to tephriphonolites. Trace element contents of Uwayrid lavas suggest they were generated by low-degree partial melting of amphibole-bearing fertile lherzolites, initially at a higher degree of melting and greater depths in the presence of residual garnets (Rumadah basalt) and progressively at a lower degree of melting and shallower depths in the spinel stability field (Jimlud basalt). Harrat Uwayrid lavas show little variability in Sr-Nd-Pb radiogenic isotopes, similar to most basalts of north-central Arabia. They have relatively enriched Pb isotopic compositions coupled with low-Sr and relatively high-Nd, and are assumed to have derived from an

ancient and enriched mantle-component within the subcontinental lithospheric mantle (Altherr et al., 2019). The base of the Uwayrid lava flows is underlain by sandstones of the Saq Formation.

Sedimentary Rocks and Tectonic Structures

The Early Ordovician Saq Sandstone is a conglomeratic, sandy and silty formation lying in conformity over older Phanerozoic sedimentary rocks. It is subdivided from the base upward into the Risha and the Sajir members (Vaslet et al., 1994). The Risha Member consists of beige to tan coarse-grained to conglomeratic sandstone with massive bedding, deposited in a braided alluvial fan and consisting of channel-fill sequences with lag gravel and prograding fluvial dunes, and with rapid channel migration. The Sajir Member overlies conformably the Risha Member reaching thickness of ~500 m in the study area. Its deposits include: 1) beige to tan coarse-grained micro-conglomeratic sandstone formed in a delta prograding environment with periodic marine onlap; 2) beige to white coarse-grained micro-conglomeratic sandstone that represents deltaic bar sediments

formed under strong marine influence; and 3) white medium to coarse grained sandstone deposited in tidal flats with tidal channels and sand fans.

Mesozoic and Cenozoic sedimentary deposits overlie unconformably the Paleozoic rocks and include: the Aruma, Mira and Ajfar formations, and Quaternary surficial sediments consisting of eolian sand, wadi and lacustrine deposits. The Late Cretaceous Aruma Formation is formed by clastic rocks including sandstone, siltstone and claystone deposited in continental environments from fluvial to flood plains. It outcrops mainly within the Tabuk graben where isolated remains have been preserved by subsequent erosion. The Mira Formation is an Early Eocene fossiliferous limestone with phosphatic and carbonate rocks deposited from nearshore to shallow water marine environments. It overlies unconformably the Aruma Formation or directly the Saq Sandstone in outcrops preserved locally within the Tabuk graben (Figure 2).

The entire stratigraphic sequence in the study area forms part of a large homocline gently dipping NNE ($<1^\circ$). This smooth homocline is dissected by a swarm of NW-SE faults, parallel to the axis of the Red Sea, named "Ribbon faults" by Roobol and Stewart (2019) because they produce long ribbon-like features. Faults and secondary sigmoid grabens result from crustal extension and show joints filled with limonite ironstone due to weathering that resists erosion to form ridges. The major structural elements of the area consist of three grabens; Tayma, Fayha and Tabuk (Figures 1, 2), that result from two distinct tectonic phases (Vaslet et al., 1994). An older phase with the formation of WNW-ESE dextral transtensional faults and large tension gashes along NNW-SSE conjugate structures, that induced the sinuous shape and angular pattern of the faults that bound the main grabens. A second stage of deformation took place during the Late Miocene and Pliocene with sinistral reactivation of the early major boundary faults.

Marthoum Volcanic Pipes

East of Harrat Uwayrid, within a 20 km by 30 km area between 27° and 27.5° N latitude and 37.5° – 38° E longitude, aligned along the NNW normal faults that divide the Phanerozoic sandstones into long narrow horst-graben stripes, over one hundred volcanic pipes intrude the sandstones occupying a stratigraphic horizon in the Saq Formation (Figures 1, 2; Liddicoat, 1982). Most of them are circular or elliptical features marked by craters aligned along NW-SE fractures in the sandstone. Craters are commonly filled with basalts that rise in conical hills resistant to erosion. The contact between the basalts and the host sandstone consists of ferruginous, satin, mylonite-breccia sandstone, a few meters thick and a colour that depends on the amount of iron oxide and hydroxide, ranging from cream to dark brown. Well-rounded quartz grains derived from the Paleozoic sandstones are the main component of this shear zone, which contains also angular fragments of silicified sandstone derived from the external zone (Vaslet et al., 1994). Adjacent to the shear zone, the country rock is silicified for a thickness of 10–100 m and therefore resistant to erosion. As a result, the basaltic core is generally surrounded by a sandstone wall or rim. Basalts show well-developed columnar joints with long narrow columns with

10–20 cm average diameter. In the central sector of the crater, the columns are vertical, while they extend sub-horizontally approaching the edges of the structure. Typically, the rock is black and glassy, free of vesicles, and very different from the holocrystalline basalts of the Uwayrid lava flows, where the columns are considerably larger.

The volcanic pipes show two distinct morphologies: most have a central basaltic core with vertical walls, and diameter commonly <300 m, and with the characteristic erosion-resistant collar of silicified sandstone (Figures 3D,E). Others (20%), despite having a sandstone collar, show little or no basalt with columnar jointing and commonly have a crater with a depressed central part and a flat bottom (Figures 3A,B). These structures are filled with chaotically oriented blocks and rafts of sedimentary rocks, mostly blocks of the Saq Sandstone, but also fossiliferous blocks of the Mira Formation with steeply inclined strata towards the center of the crater. These volcanic structures, lacking the central core of basalt with columnar jointing, can be associated with explosive pyroclastic activity and with the formation of maars. The filling of sedimentary blocks derived from higher stratigraphic levels is probably the result of the collapse of the maar walls into the crater. Thus, only these pipes can be considered diatremes (Liddicoat, 1982).

The emplacement of these structures within the Saq Sandstone and the chilled, vitrified nature of the basalts suggest that the pipes are the result of phreatomagmatic explosions that occurred when rising magma met the water table in the porous sandstone host (Figures 3C,F). However, the level of erosion is such that all surface deposits are now completely removed. Most of the pipes that have a core of columnar basalts can be considered eroded feeder conduits to diatremes. The elevation of these structures, greater than that of the base of the Uwayrid lava flows, suggests that their formation, occurred when the erosion level of the Phanerozoic rocks was higher, before the Uwayrid related magmatism in the area (Vaslet et al., 1994).

DATA AND METHODS

We conducted fieldwork and sampling on a representative subset of Uwayrid lava flows in the spring of 2016 (Figure 1). Within the study area, the volcanic activity is represented by two principal groups: 1) lavas exposed on Harrat Uwayrid consisting of a sequence of flat lying, mainly alkali-olivine basalt flows; and 2) basalts from volcanic pipes/diatremes intruding the Saq Sandstone immediately to the east of Uwayrid (Marthoum area), ~60 km north-northwest of Al'Ula (Figures 1, 2). Samples from Uwayrid were collected from different volcanic units [Tr₁-Tr₂ to Qj₁-Qj₄ of Vaslet et al. (1994)] at sampling sites specifically selected to supplement previous sampling by Altherr et al. (2019). The adopted sample names (UH-xx/SampleName) provide information on sampling site (xx), presumed age of the volcanic unit or pipe rock (Qb, Tb, and Pi: Quaternary, Tertiary and pipe basalt) and sample number. Geochemical and isotopic analyses, and K-Ar dating on selected samples were performed at Activation Laboratories Ltd. (Ancaster, Ontario; www.actlabs.com).

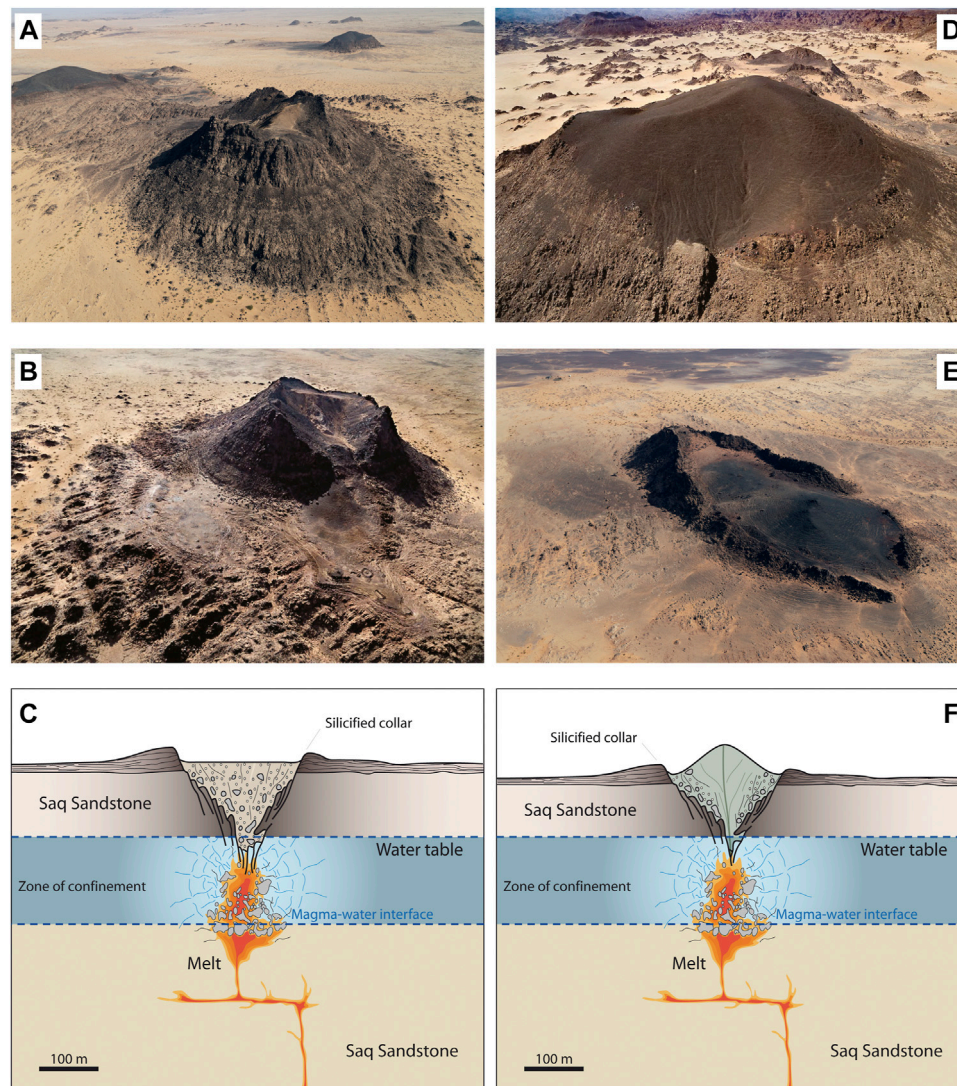


FIGURE 3 | Aerial view of the Marthoum volcanic pipes without (A,B) and with (D,E) intra-crater columnar-jointed basalt surrounded by a collar of silicified Paleozoic sandstone. Location of pipes in (A, B, D, E) is shown in Figure 1. UH-10 samples are from the pipe shown in (D). (C,F) cartoons showing pipe formation mechanism by generalized sections through the main pipe/crater types identified.

Major and Trace Elements Geochemistry

A subset of 37 samples (32 from Uwayrid and five from Marthoum pipes) were selected for geochemical analyses, based on stratigraphy and texture. To minimize the effect of alteration, samples were selected from the innermost portion of the basaltic flows with minimal number of vesicles. Details of sample locations are presented in Figure 1 and in Supplementary Table S1. Selected portions (sub-samples) of each sample were crushed and pulverized in a tungsten carbide swing mill and measured for major and trace element concentrations using Inductively Coupled Plasma Optical Emission Spectroscopy (ICP-OES) and ICP Mass Spectrometry (ICP-MS). Results are reported in Supplementary Table S1. Total uncertainties of the element analyses are generally within 10%.

K-Ar Age Determinations

Two samples (UH-05/Pi-1a and UH-10/Pi-3) from the Marthoum pipes were selected for K-Ar dating (Table 1). Samples were pulverized and weighed in an aluminium container, loaded into the extraction unit sampling system and degassed at $\sim 100^{\circ}\text{C}$ for 2 days to remove surface gases. Argon was extracted from the sample in a double vacuum furnace at $1,700^{\circ}\text{C}$. The determination of radiogenic argon content was carried out twice on a MI-1201 IG mass-spectrometer by an isotope dilution method with ^{38}Ar as a spike, introduced to the sample system prior to each extraction. The extracted gases were cleaned up in a two-step purification system. Pure Ar was successively introduced into a custom-built magnetic sector mass spectrometer (Reinolds-type). Tests were repeated twice per sample to ensure consistency of results. Two globally accepted

TABLE 1 | Bulk rock Sr, Nd, Pb and Hf isotopic contents and K-Ar dates of selected Marthoum pipes.

Sample	UH-05/Pi-1a			UH-10/Pi-3				
	Volcanic pipes							
	Bulk	$\pm 2\sigma$	Bulk ^a	Groundmass	$\pm 2\sigma$	Bulk	$\pm 2\sigma$	Bulk ^a
⁸⁷ Sr/ ⁸⁶ Sr	0.70343	0.00002	0.70337			0.70320	0.00002	0.70311
¹⁴³ Nd/ ¹⁴⁴ Nd	0.51275	0.00001	0.51271			0.51280	0.00001	0.51274
ϵ_{Nd}	2.26		2.72			3.24		3.81
²⁰⁶ Pb/ ²⁰⁴ Pb	20.153	0.001	19.897			19.853	0.001	19.462
²⁰⁷ Pb/ ²⁰⁴ Pb	15.687	0.001	15.675			15.655	0.001	15.636
²⁰⁸ Pb/ ²⁰⁴ Pb	40.021	0.004	39.735			39.577	0.003	39.140
¹⁷⁶ Hf/ ¹⁷⁷ Hf	0.282788	0.000003	0.282783			0.282738	0.000006	0.282730
ϵ_{Hf}	0.57		1.49			-1.20		0.04
K (wt%)	1.67	0.02		1.59	0.02	1.02	0.02	
⁴⁰ Ar _{rad} (ng/g)	5.963	0.023		5.870	0.060	5.082	0.019	
⁴⁰ Ar _{atm} (ng/g)	14.20			39.60		11.70		
Age (Ma)	50.7	1.3		52.5	1.5	70.5	2.5	

^aThe initial isotopic ratios are calculated at 50 Ma (UH-05/Pi-1a) and at 70 Ma (UH-10/Pi-3) using the natural abundances of parent-daughter isotopes. 2σ uncertainties represent the 95% confidence interval.

standards (Bern-4M Muscovite and 1/65 “Asia” rhyolite matrix) were measured for ³⁸Ar spike calibration. Age calculations are based on the following international values of constants: $\lambda_K = 0.581 \times 10^{-10} \text{ a}^{-1}$, $\lambda_{\beta^-} = 4.962 \times 10^{-10} \text{ a}^{-1}$, $^{40}\text{K} = 0.01167$ (at.%), where λ_K is the decay constant of the first-order reaction transforming ⁴⁰K into ⁴⁰Ar, λ_{β^-} is the decay constant producing ⁴⁰Ca and ⁴⁰K is the fractional isotopic abundance.

Pb-Nd-Sr-Hf Isotopic Analysis

Aliquots of the two samples from the Marthoum pipes used for age determinations were powdered and subjected to Pb, Sr, Nd and Hf isotopic analyses (Table 1).

Sr isotopes: the rock powders were dissolved in HF + HNO₃ at 150°C for 5 days, and chemical separation procedures for Sr follow the methodology of Creaser et al. (2004) and Holmden et al. (1997). All analyses are presented relative to a value of 0.710245 for the SRM987 Sr isotopic standard.

Nd isotopes: sample dissolution was in HF + HNO₃ at 150°C for 5 days, and following chemical separation procedures outlined by Creaser et al. (1997) and Unterschutz et al. (2002), the isotopic analysis was conducted by MC-ICP-MS (Schmidberger et al., 2007). The fluoride residue is converted to chloride with HCl, and Nd and Sm are separated by conventional cation and HDEHP-based chromatography. Chemical processing blanks are <200 pg of either Sm or Nd, and are insignificant relative to the amount of Sm or Nd analysed for any rock sample. The Geological Survey of Japan Nd isotope standard “Shin Etsu: J-Ndi-1” (Tanaka et al., 2000) was analysed for calibration. J-Ndi-1 standard has a ¹⁴³Nd/¹⁴⁴Nd value of 0.512107 ± 7 relative to a LaJolla ¹⁴³Nd/¹⁴⁴Nd value of 0.511850, when normalized to ¹⁴⁶Nd/¹⁴⁴Nd = 0.7219. The value of ¹⁴³Nd/¹⁴⁴Nd determined for the J-Ndi-1 standard during the analysis was 0.512096 ± 6 (2σ). ϵ_{Nd_0} is the epsilon ¹⁴³Nd value calculated for the present day.

Pb isotopes: sample powders were dissolved in ultrapure HF + HNO₃ at 100°C for 2 days. Sample solutions were then evaporated under UPLA-filtered air, and converted to chlorides using 6N HCl, and bromides using 2N HBr. Lead was purified by standard anion exchange chromatography using HBr and HNO₃ as eluents

under UPLA-filtered conditions. The isotopic composition of Pb was then measured by MC-ICPMS in static analysis mode. The measured Pb isotope ratios were corrected for instrumental mass bias using the agreed value for ²⁰³Tl/²⁰⁵Tl ratio measured simultaneously with each Pb analysis (e.g., Belshaw et al., 1998). Overall reproducibility of any Pb isotope measurement is based on > 6 years of analyses of SRM981 Pb isotope standard. The most widely accepted values for this Pb isotope standard are those determined by Todt et al. (1996) by double-spiked TIMS analysis, which are: ²⁰⁶Pb/²⁰⁴Pb = 16.936; ²⁰⁷Pb/²⁰⁴Pb = 15.489; ²⁰⁸Pb/²⁰⁴Pb = 36.701. All Pb isotope data reported in Table 1 are normalized to the values of Todt et al. (1996).

Hf isotopes: analysis was conducted on the unleached rock powder by MC-ICPMS following the method of Blichert-Toft and Albarede (1997). During the analysis two sets of standards were measured: JMC475 and BHVO.

Rock Magnetic Properties and Paleomagnetism

Five hand samples (AR138-142) were collected from the Marthoum pipes for magnetic analyses. Sample orientations were obtained using a magnetic compass in the field. Between 1 and 5 standard paleomagnetic cylinders of 2.54 in diameter and 2.2 cm in height were drilled in the laboratory from each rock sample for a total of 10 samples analyzed. The Natural Remanent Magnetization (NRM) was measured using a SPM spinner magnetometer at the Paleomagnetic Laboratory of ISMAR-CNR in Bologna (Italy). Both the alternating field (AF) (up to 60 mT) and the thermal demagnetization (up to 540°C) were carried out on pilot samples to verify their reliability and magnetic behaviour during cleaning. Stepwise AF demagnetization was applied using an AGICO LDA-3A demagnetizer, while a MMTD1 furnace was used for thermal demagnetization. The results were analysed by using the DAIE program (Sagnotti, 2013) based on Fisher statistics (Fisher, 1953) and principal component analysis (Kirshvink, 1980). A FORC diagram was measured at the INGV paleomagnetic laboratory in

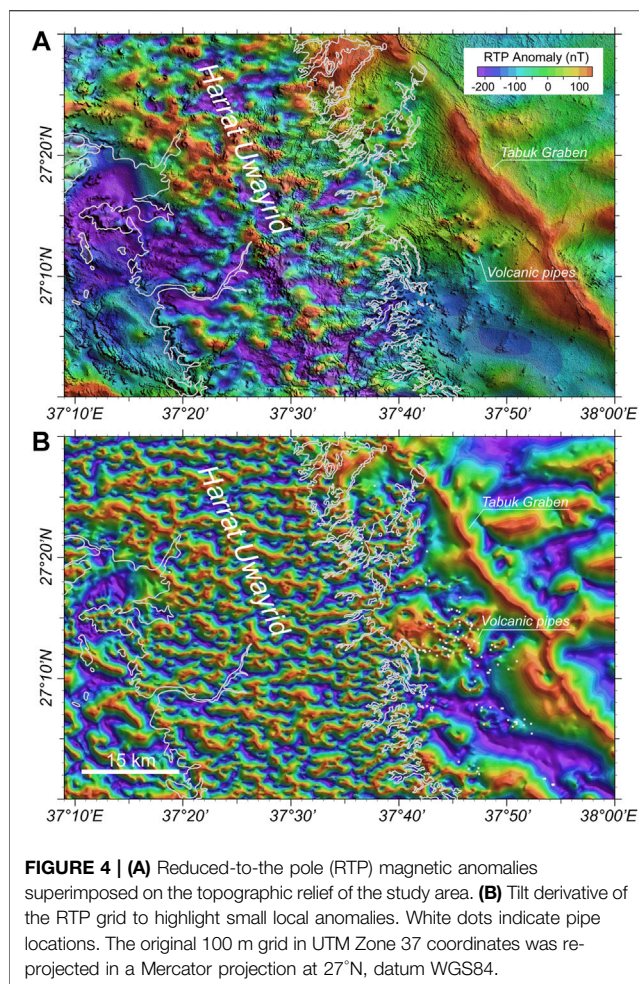


FIGURE 4 | (A) Reduced-to-the pole (RTP) magnetic anomalies superimposed on the topographic relief of the study area. **(B)** Tilt derivative of the RTP grid to highlight small local anomalies. White dots indicate pipe locations. The original 100 m grid in UTM Zone 37 coordinates was re-projected in a Mercator projection at 27°N, datum WGS84.

Rome using a Micromag alternating gradient magnetometer (AGM-2900) with a maximum field of 1 T. The Isothermal Remanent Magnetization (IRM) was imparted to one sample (AR140-bl) in 25 steps between 0.003 and 1 T using an ASC IM-30 pulse magnetizer and the coercivity spectrum was evaluated using MAX UnMix software (Maxbauer et al., 2016).

Aeromagnetic Data

Due to their magnetic mineral content the pipes may be expected to have some expression in the magnetic anomaly field, as shown in **Figure 4**, which is based on the compilation and grids of the available aeromagnetic surveys summarised by Zahran et al. (2003). The 1981 aeromagnetic survey over the harrat was flown with a line spacing of 2,000 and 500 m altitude, in a direction 45°N. The 1962 survey in the shield outside the harrat to the west was at 800 m line spacing and 300 m height, at 30°N. The data to the east of the harrat is from a survey flown in 1983 on N-S lines at 2,000 m spacing and 120 m altitude (Phoenix Corporation, 1985). The data are shown here on a 100 m grid in order to retain detail along the flight lines. Since the field inclination was about 39° from horizontal, reduction to the pole (RTP) was carried out using the usual Fourier methods in order to place anomalies over their causative sources. The

resulting RTP image (units in nT) is shown in **Figure 4A**, where shading is by illumination from the NE.

RESULTS

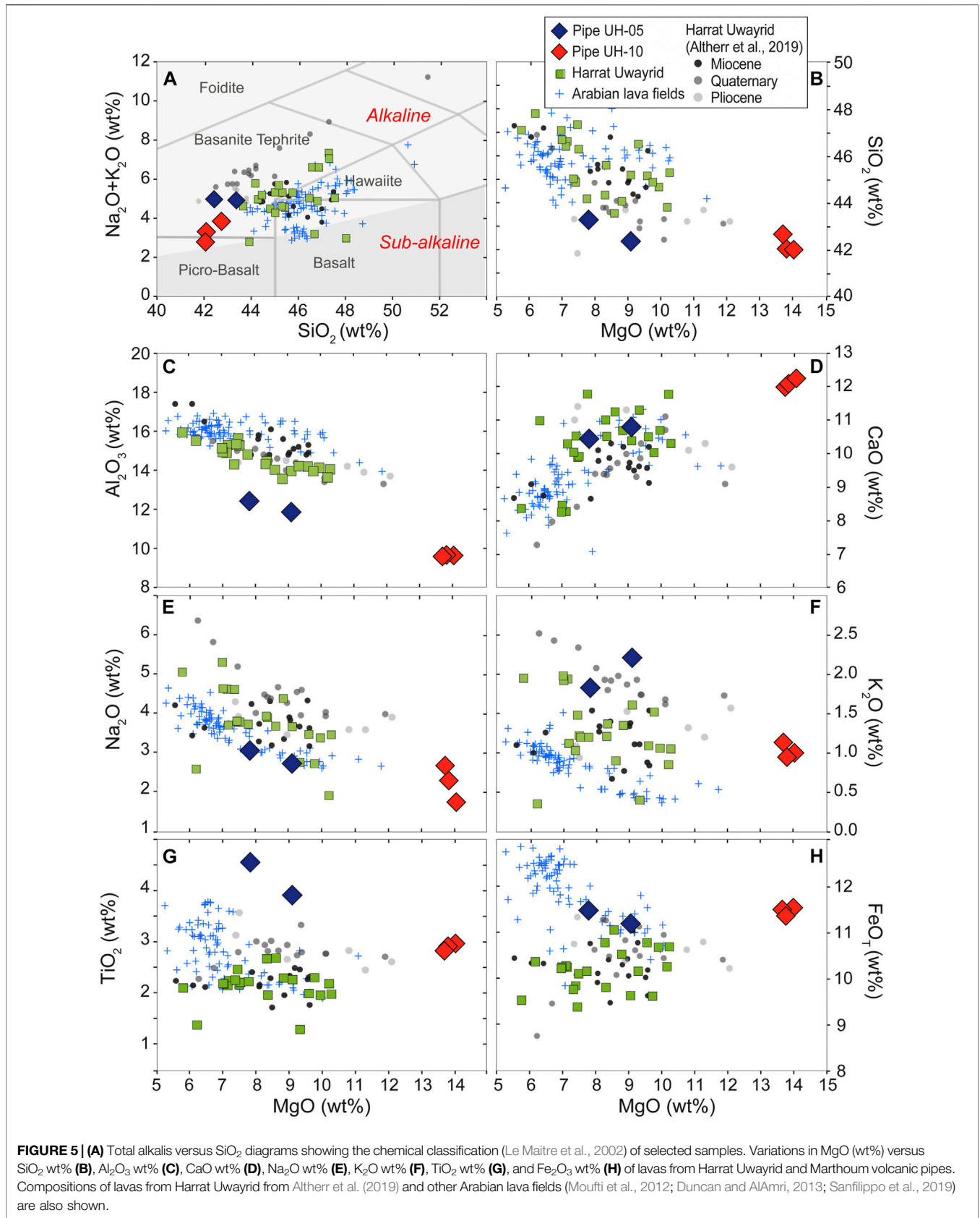
Petrology and Geochemistry of Uwayrid Basalts

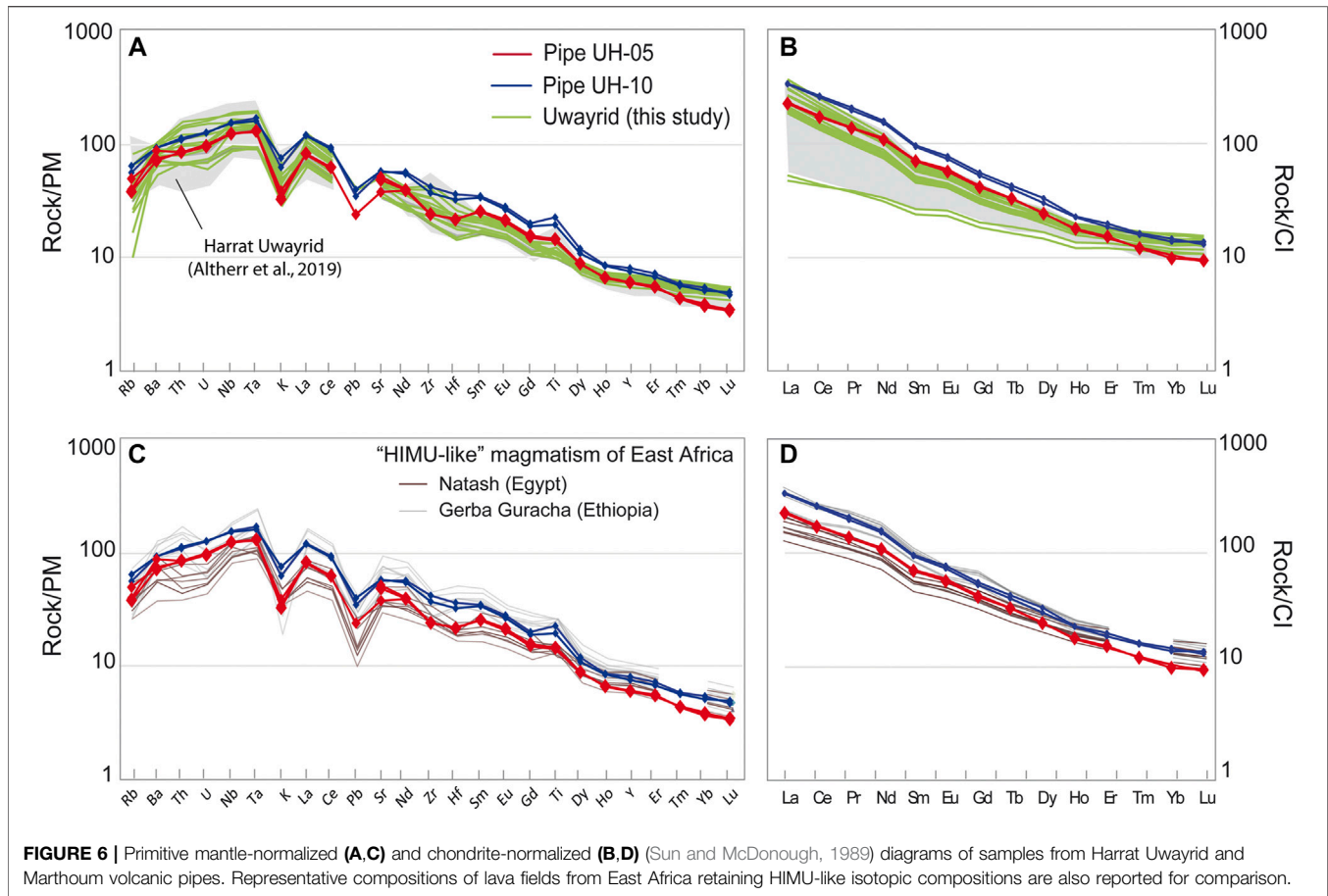
The collected rocks from Harrat Uwayrid are alkaline-olivine basalts and fall into the field of basalts, hawaiiite and basanite with SiO₂ ranging within 42–48 wt%. Most of the basalts have a porphyritic texture with up to 20 vol% phenocrysts consisting of fresh olivine (50–60%), clinopyroxene (20–30%) and oxides (5–10%) dispersed in a glassy matrix. Phenocrysts of clinopyroxenes commonly create mm-scale polycrystalline aggregates. Plagioclase is nearly absent as phenocryst, but locally shows flow-induced alignments within the groundmass. Mantle and lower crust xenoliths are present locally in the Uwayrid lavas, consisting mainly of spinel lherzolite, websterite and a subset of mafic lithologies ranging from troctolite to olivine gabbro (Kaliwoda et al., 2007).

Uwayrid basalts range from primitive to relatively evolved compositions having MgO contents between 10.5 and 5.5 wt%. As a result of fractional crystallization of olivine and clinopyroxene, the rock samples show decreasing MgO at increasing SiO₂, Al₂O₃ and most of the incompatible elements (Na₂O, P₂O₃), whereas CaO, K₂O, TiO₂ and FeO contents are highly scattered with no discernible trend (**Figure 5** and **Supplementary Table S1**). Compatible trace elements such as Ni (80–230 ppm) and Cr (100–450 ppm) are positively correlated with MgO in all samples, reflecting olivine, spinel and clinopyroxene fractionation. Incompatible trace elements in analysed samples normalized with respect to primitive mantle (PM) composition display the typical pattern of alkaline basalts of western Arabian lavas (**Figure 6A**). They have negative Pb and K anomalies and low content of large-ion lithophile elements (LILE, e.g., Rb and Ba) when compared to the neighbouring elements (**Figure 6A**). Overall, trace element compositions show a very steep negative slope from Ta to Lu and positive slopes from Rb to Nb and Rare Earth Elements (REE) gradually decreasing from light REE (LREE) towards heavy REE (HREE) (**Supplementary Table S1**). The chondrite-normalized REE patterns show the typical LREE enrichment of Arabian intra-plate volcanism (Coleman et al., 1983; Moufti et al., 2012; Duncan and Al-Amri, 2013; Altherr et al., 2019; Sanfilippo et al., 2019) with (La/Yb)_n ranging from 14.50 to 22.5 and are variably fractionated in MREE/HREE with (Gd/Yb)_n ranging from 2.2 to 2.7 (**Figure 6B**).

Petrology and Geochemistry, K-Ar Dating and Rock Magnetism of Marthoum Pipes

Petrology and geochemistry: rock samples from the Marthoum pipes include black, very fine-grained, low vesicular basalts with a porphyritic or glass-fibre texture and containing olivine and olivine-clinopyroxene assemblages with unusually little plagioclase. Large phenocrysts of olivine and clinopyroxene are



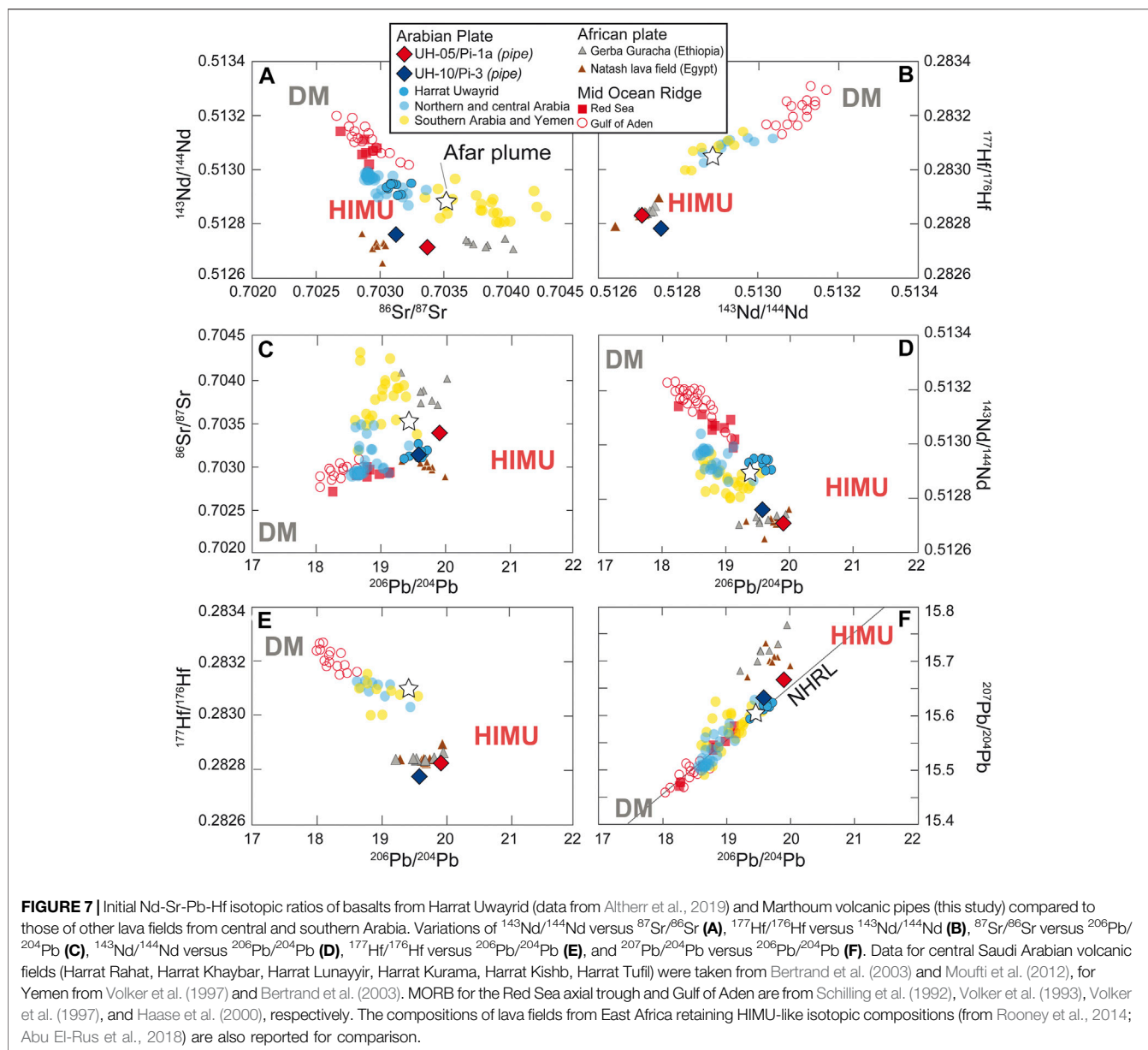


dispersed in a fine-grained groundmass consisting of olivine, pyroxene, magnetite and traces of calcic plagioclase. The main mineralogical phases are 50–60% olivine, 20–30% pyroxenes and 5–15% Ti-Fe oxides. Olivine phenocrysts are commonly euhedral, colourless and slightly elongated in thin sections. The crystals are commonly crossed by fractures and are partially altered and replaced with fine-grained assemblages of clay minerals (~10–15%). Pyroxenes are colourless in thin sections, with a slight pleochroism and a granular prismatic habit. Typically, euhedral pyroxenes have a corroded core, showing a prominent sieve texture and a distinctly zoned outer margin suggesting local dissolution during the melt ascent. Some samples have sparsely distributed rounded xenocrysts of polycrystalline quartz derived from wall-rocks and showing magmatic corrosion reaction rims.

The analysed samples fall within the basanite field with transition to picro-basalts with a MgO content of up to ~14 wt % at site UH-10 (Figure 5A). The lavas from the Marthoum pipes show different major element compositions compared to those of Harrat Uwayrid, having lower SiO₂ (42–43.5 wt%) and Al₂O₃ (9–13 wt%) and higher TiO₂ (3–4.7 wt%) and FeO (11–11.6 wt%) contents ((Figure 5 and Supplementary Table S1). Ni and Cr contents are also extremely high, indicative of their primitive character (Supplementary Table S1). The high-field-strength elements (HFSE) contents differ

from those of the Uwayrid lavas and reveal a higher Ti anomaly and a Zr and Hf depletion when compared to the neighbouring trace elements in a PM-normalized spider diagram (Figures 6A,C). Chondrite-normalized REE contents of the Marthoum pipes reveal a higher fractionation of MREE/HREE than the Uwayrid basalts with (Gd/Yb)_n ranging from 3.7 to 4.3 and similar LREE/MREE ratios (Figures 6B,D).

Sr-Nd-Hf-Pb isotopic determinations were carried out on two samples from the Marthoum pipes. Isotopic ratios were corrected using their measured K-Ar ages, although they are nearly indistinguishable from present-day compositions (Table 1). Initial isotopic compositions show low ¹⁴³Nd/¹⁴⁴Nd (0.512713–0.512761) and ¹⁷⁶Hf/¹⁷⁷Hf (0.28273–0.28278), relatively low ⁸⁷Sr/⁸⁶Sr (0.70312–0.70336), and strongly radiogenic ²⁰⁶Pb/²⁰⁴Pb (19.57–19.90), ²⁰⁷Pb/²⁰⁴Pb (15.67–15.64) and ²⁰⁸Pb/²⁰⁴Pb (39.26–39.73). Compared to the basalts from the nearby Harrat Uwayrid (Altherr et al., 2019), volcanic pipes have more radiogenic Pb isotope ratios, lower Nd but similar Sr isotope contents. In addition, their isotopic compositions are also clearly distinct from those of Afar Plume magmatism having markedly lower Sr, Nd and Hf, and higher Pb isotopic ratios (Figure 7). On the other hand, the Marthoum pipes display isotope ratios similar to those of HIMU-like lava fields of East Africa, i.e., Natash, western Egypt and

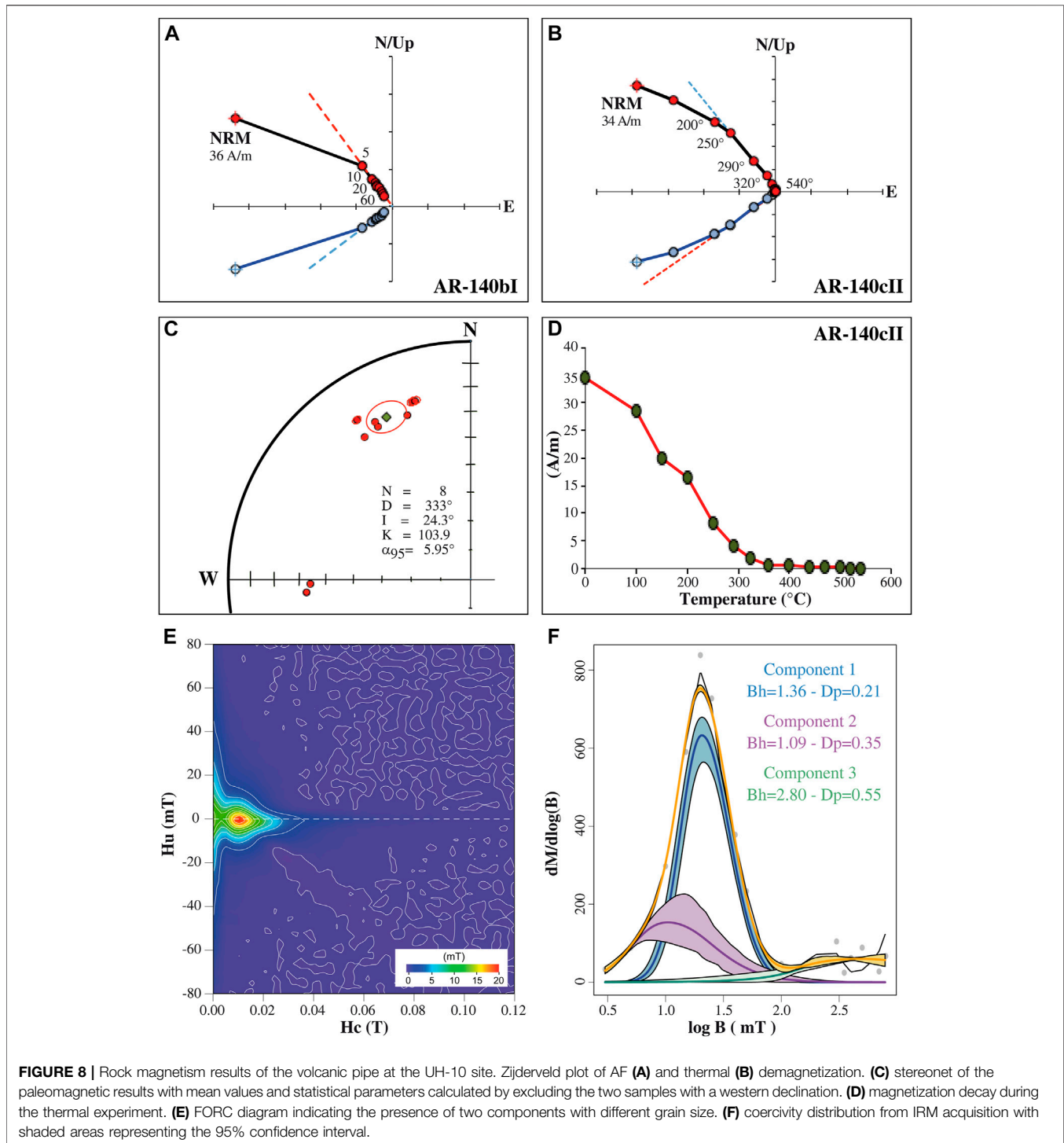


Gerba Guracha, Ethiopia (Rooney et al., 2014; Abu El-Rus et al., 2018).

K-Ar age determinations: based on a low LOI two columnar basalt samples without macroscopic evidence of alterations were selected for K-Ar isotopic age determinations on bulk-rock separates, resulting in a Late Cretaceous age of 70.5 ± 2.5 Ma (UH-10/Pi-1a) and an Early Eocene age of 50.7 ± 1.3 Ma (UH-05/Pi-3) (Table 1). Sample UH-05/Pi-1a contains few quartz xenocrysts in thin section, hence K-Ar dating was repeated on the glassy groundmass to overcome possible crustal contamination. Groundmass dating provided an age of 52.5 ± 1.5 Ma comparable with the value determined from the bulk-rock (Table 1). Our new ages agree with observations of Vaslet et al. (1994) that the volcanic pipes are older than exposed Rumadah lava flows that crops out nearby, because they lay in

sandstone at a higher level than the erosional surface underlying the base of the adjacent basalts. However, our findings are in contrast with the idea that the basaltic pipes are contemporary with the early stage of Uwayrid volcanism (Middle Miocene; Liddicoat, 1982).

Rock magnetism: columnar basalts from the volcanic pipe at site UH-10 (Figure 1) have also been investigated for magnetic properties and paleomagnetism. The intensity of magnetization of the samples is high and scattered between 12 and 79 A/m. AF cleaning, used to demagnetize the rock samples, shows a secondary overprint that affects mainly the magnetic declination. This secondary magnetization is removed after applying a field of 10–15 mT or a temperature of 150–200°C, after which its direction stabilizes toward a stable vector representing the Characteristic Remanent Magnetization



(ChRM) (Figures 8A,B). Following the application of an AF of 5–10 mT magnetic field, the intensity of magnetization rapidly decreases with the median destructive field (MDF) of NRM ranging between 3.9 and 13.7 mT. The above suggests that lightning strikes may be a cause of the observed high intensity of magnetization, also considering that the secondary component is larger in the more resistant samples. The two specimens from

the sample with the highest magnetization (sample AR141: $J = 78\text{--}79$ A/m) exhibit a ChRM with a western declination ($D = 267^\circ$, $I = 34^\circ$) not consistent with the mean value of all the other samples ($D = 333^\circ$, $I = 24.3^\circ$, Figure 8C). This average value, although it has some dispersion ($K = 103.9$ and $\alpha_{95} = 5.95^\circ$ for the eight samples), can be considered representative of the Earth's magnetic field at the time of the pipe formation. Results

indicate a counterclockwise rotation and a lower paleo-latitude of the Arabian Plate at the time of emplacement of the rocks, in agreement with the reconstructed kinematics of Arabia during the Tertiary (Vigliotti et al., 2019 and references therein). The total rotation angle of $\sim 27^\circ$ is larger than the value obtained from Tertiary volcanic rocks; however, it may be within the range of secular variations, not mediated by measurements of a single magmatic event.

The main carrier of remanent magnetization is titanomagnetite with a consistent amount of Ti, as indicated by the decrease of magnetization during thermal cleaning, with most of the magnetization lost below 300°C (Figure 8D). Paleomagnetic data show a consistent normal polarity that can be correlated with the Chronostratigraphic Time Scale (Ogg, 2012) within the time interval provided by the K-Ar dating (68–73 Ma). The correlation suggests an emplacement of the pipe at site UH-10 within Chron C31n (68.369–69.269 Ma) or C32n-1n/2n (71.449–71.689/71.939–73.649 Ma).

First-order reversal curve (FORC) diagrams provide an insight into the state of the magnetic domain of particles. The FORC diagram of sample AR140-bI shows evidence of mixing of pseudo-single-domain (PSD)-like and multi-domain (MD)-like magnetic moments (Figure 8E). The presence of PSD-like moments is documented by the closed contour lines, while the dispersion around the magnetic induction (B_u) axis indicates the MD grains. In addition, the divergence of the closed contours toward the intrinsic induction (B_i) axis indicates magnetostatic interactions of grains (Roberts et al., 2000). UnMix results of isothermal remanent magnetization (IRM) reveals that the coercivity spectrum can be described by a three components model with two nearly overlapping low coercivity components (Figure 8F). The first low coercivity component₁ has a B_h (coercivity) of 1.35 (+/- 0.011) log₁₀ units (22.7 mT) and a DP (dispersion parameter) of 0.21 (+/- 0.005); the second low component₂ has a B_h of 1.098 (+/- 0.048) log₁₀ units (12.5 mT) and a DP of 0.35 (+/- 0.036), whereas the high coercivity component has a B_h of 2.8 (+/- 0.14) log₁₀ units (633.3 mT) and a DP of 0.55 (+/- 0.12) (Figure 8F). The low-coercivity components can be related to a single mineral phase, such as titanomagnetite, with grains of different size as shown in the FORC diagram (Figure 8E).

Magnetic anomalies: the anomaly field in Figure 4A is somewhat chaotic over Harrat Uwayrid, which is typical of all the Arabian lava fields (Stern and Johnson, 2010). The prominent linear positive anomaly trending NW-SE toward the right side of the image is related to the great Jada'ah dike (Phoenix Corporation, 1985) that extends to the Dead Sea fault zone in Jordan (Hatcher et al., 1981), but is exposed only in a few places in Jordan (Johnson and Vranas, 1992). Generally, the dike could be several hundred metres wide, but with few outcrops (cf. Red Sea coastal dikes; Blank, 1977; Roobol and Stewart, 2019). The intrusion of this near-vertical mafic dike may have favoured the formation of the superficial Tabuk graben (Chadwick and Embley, 1998). It has also been suggested (Vaslet et al., 1994) that the strong magnetic anomaly is linked to the alteration of the Saq sandstones due to fluids circulating along fault planes of the Tabuk graben with the formation of a thick layer (although only

up to tens of metres wide) of dark, dense and silicified iron oxides and hydroxides (goethite); a fault that is sufficiently coated at depth by these ferromagnetic oxides could generate some of the observed magnetic anomalies.

In order to highlight the smaller magnetic features, the tilt derivative of the RTP field is shown in Figure 4B, which includes the locations of the pipes; this is a geometrical function of the horizontal and vertical derivatives and acts as a type of automatic gain control (AGC), thus enhancing the short-wavelength low-amplitude anomalies. From Figure 4B it can be seen that the pipes tend to be associated with local anomalies, and possibly even with very local lineations.

DISCUSSION

Fractional Crystallization and Crustal Assimilation Processes

Basalts from the Harrat Uwayrid and Marthoum pipes show large compositional variations of major and trace elements suggesting melts generated by partial melting of a composite mantle source. In agreement with previous results (Altherr et al., 2019), the analysed Uwayrid rocks display a variety of evolved compositions (MgO 5–10 wt%) with good consistency between lavas of different ages as shown by Altherr et al. (2019) (Figure 5). Covariations of MgO with other major elements define local fractionation trends, suggesting an origin from geochemically similar parental melts. For instance, the most primitive Uwayrid lavas display a gradual increase of CaO from 9 to 11 wt% with a decrease of MgO from 12 to 9 wt%, while CaO in lavas with MgO contents lower than 9 wt% decreases as MgO, reaching the minimum value of 7 wt% in the most evolved rocks (Figure 5D and Supplementary Table S1). In contrast, Al₂O₃ gradually increases with decreasing MgO in all the lavas (Figure 5C and Supplementary Table S1), leading to a gradual decrease in CaO/Al₂O₃ ratio with decreasing MgO, similar to other lava field basalts in the region (Moufti et al., 2012; Duncan and Al-Amri, 2013; Sanfilippo et al., 2019). This suggests crystallization of olivine and clinopyroxene followed by plagioclase, only in those lavas that have a MgO content as low as 4 wt%. The early crystallization of olivine and clinopyroxene agrees with the presence of these phases as phenocrysts and the absence of plagioclase. Geochemically, there are notable differences between Uwayrid basalts, and adjacent ones extruded as volcanic pipes. Despite the limited variety of the sampled volcanic pipes, their columnar basalts range from very primitive to more evolved compositions and trace a slightly different evolutionary trend compared to the Uwayrid lavas (Figure 5). For instance, the basalts of the pipes define an MgO vs. Al₂O₃ trend parallel to those of the Uwayrid lavas but at constantly lower Al₂O₃ (<13 wt%). Another important difference is the TiO₂ content, which in the volcanic pipes is consistently higher than in the Uwayrid lavas, indicating that the pipes were formed by injection of a primary melt strongly enriched in TiO₂ (>3 wt%). The high Ti content is also supported by paleomagnetic data indicating that most of the magnetization is lost at <300°C (Figure 8D); a clear indication of

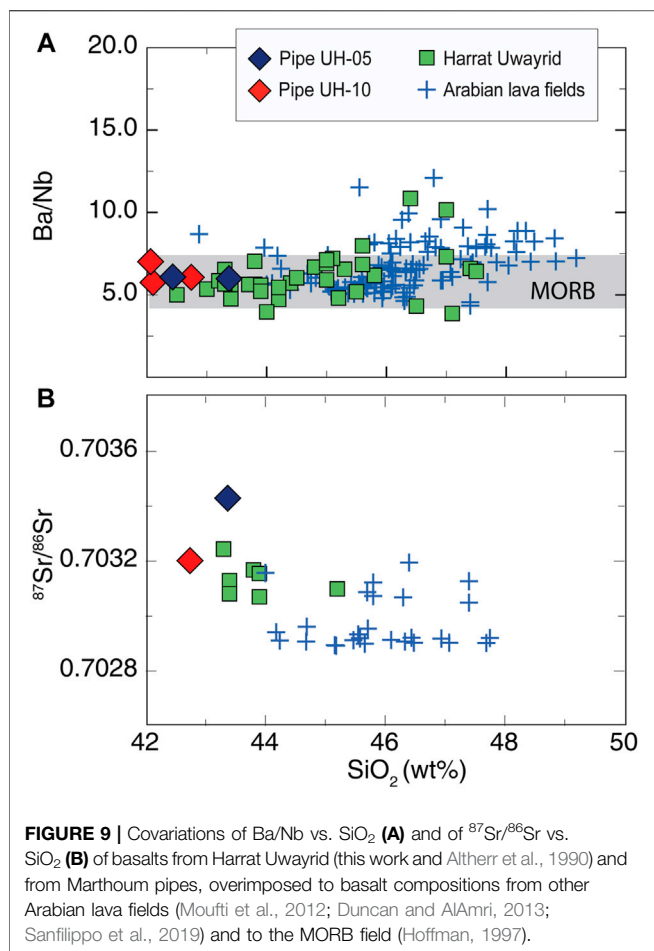


FIGURE 9 | Covariations of Ba/Nb vs. SiO₂ (A) and of ⁸⁷Sr/⁸⁶Sr vs. SiO₂ (B) of basalts from Harrat Uwayrid (this work and Altherr et al., 1990) and from Marthoum pipes, overimposed to basalt compositions from other Arabian lava fields (Moufti et al., 2012; Duncan and AlAmri, 2013; Sanfilippo et al., 2019) and to the MORB field (Hoffman, 1997).

significant Ti substitution within titanomagnetite. Ti-rich primary melts as those with Ti anomaly in the PM-normalized spider diagram of Figures 6A,C, probably favoured the accumulation of the abundant oxides present in these rocks. Taken together, the evolutionary trends of the Uwayrid lavas and volcanic pipes suggest the occurrence of slightly different parental melts that followed a chemical evolution mostly driven by olivine and clinopyroxene fractionation. Fractional crystallization experiments and thermodynamic calculations show that at high pressure, clinopyroxene crystallizes before plagioclase (Presnall et al., 1978; Tormey et al., 1987; Grove et al., 1992; Yang et al., 1996), further enhanced by the alkaline nature of some of these lavas. Early crystallization of clinopyroxene has been inferred for nearly all Saudi Arabian lava fields and suggests that chemical differentiation of the primary magmas occurred in relatively deep magma chambers, within the upper mantle or at the crust-mantle boundary (Moufti et al., 2012; Duncan and AlAmri, 2013; Duncan et al., 2016; Sanfilippo et al., 2019). Crustal contamination is absent in all the basalts, as suggested by the lack of increases in elements with affinity to the continental crust. All basalts have Nb/U ratio ranging from 33 to 68, consistent with the value of 47 ± 10 for oceanic basalts (Hofmann et al., 1986). In our rocks there are no selective enrichments in large ion lithophile elements compared to high field strength elements, as evidenced

by the low Ba/Nb ratios without systematic variations with SiO₂ and with values similar to other uncontaminated lavas from Arabian and to MORB (Figure 9A). Furthermore, Uwayrid and volcanic pipes lavas have non-radiogenic Sr isotopes ($0.7031 < ^{87}\text{Sr}/^{86}\text{Sr} < 0.7033$) compared to the isotopic composition of the continental crust ($^{87}\text{Sr}/^{86}\text{Sr} > 0.706$), with the most radiogenic values having the lowest SiO₂ (Figure 9B). The absence of crustal assimilation is further suggested by the widespread occurrence of large (up to decimeter in size) mantle and lower crust xenoliths, which require a rapid rise of magma from the source region to the surface through open conduits without interactions with the host rocks.

Mantle Sources of Uwayrid and Marthoum Magmatism

As shown in the previous section, volcanic pipes and Uwayrid lavas experienced some degrees of fractionation within a deep magma chamber. Despite the paucity of samples from the Marthoum pipes, minor differences in their fractionation trend reveal primary melts having lower Al₂O₃ and high Ti contents compared with those of Uwayrid. An origin from slightly different parental melts is also evident from trace element compositions of the two series. Both are characterized by variably fractionated REE and by enrichments in incompatible elements culminating in high Nb and Ta and strongly negative Pb and K anomalies. The LILE (Rb, Ba, Cs) and, Th and U are relatively low compared to Nb and Ta. The low LILE relative to HFSE and REE contents reveal OIB-like enriched incompatible trace element patterns (Figure 6) suggesting an enriched mantle source relative to a depleted mantle (DM). The PM-normalized patterns for both series show positive anomalies in Nb, Ta and Ti and relatively low Rb, U and Th (Figure 6; Ba/Rb = 15–38 and Nb/Th = 10–16), which may reflect high Ba/Rb and Nb/Th ratios of the mantle source. Along with a pronounced negative K anomaly, these chemical characteristics can be related to the occurrence of an alkali-bearing phase, such as amphibole or phlogopite, in the mantle source. Given the high Na₂O/K₂O ratio in all samples (1.68–4.02), the occurrence of pargasitic amphibole is more plausible (e.g., Rosenthal et al., 2009) as proposed for other Saudi Arabian lava fields (NaO/K₂O = 1–7, Ba/Rb = 10–60, Nb/Th = 10–20; Moufti et al., 2013; Rooney et al., 2014; Abu El-Rus and Rooney, 2017; Altherr et al., 2019; Sanfilippo et al., 2019).

A notable difference between the pipe basalts and the Uwayrid lavas is that the former have strongly depleted HREE relative to MREE, and low Zr and Hf compared to the neighbouring trace elements (Figures 6A,B). The compatibility of HREE in garnet (Green et al., 2000) allows the use of M/HREE ratios (e.g., Gd/Yb) to infer a possible presence of residual garnets in the mantle source, which in turn depends on the melting pressure. The high Gd/Yb ratio of pipe rocks indicates residual garnet in their source; at the same time, garnet preferentially retains Zr and Hf over MREE contents, and may have caused depletion of Zr and Hf (i.e., Dalou et al., 2009). A local decrease in HREE is also documented in some of the Uwayrid lavas, where M/HREE ratios are correlated with enrichments in LREE contents

(i.e., La/Yb vs Gd/Yb). These correlations also require garnet as a buffer for HREE, an effect more efficient at low degrees of melting. The compositions of Uwayrid lavas therefore indicate an inverse correlation between the average melting pressure and the degree of mantle melting, which is common in basalts generated in an extensional setting (see also Duncan and Al-Amri, 2013; Sanfilippo et al., 2019). Hence, our results are in agreement with Altherr et al. (2019) who suggested that the Uwayrid lavas are generated by the mixing of primary melts deriving from an enriched lithospheric source that has undergone partial melting at different pressures and having either garnet or spinel as residual phases. In this context, the mantle source of the volcanic pipes appears to be located entirely in the garnet stability field with minor, if any, contribution of melt from a spinel-peridotite. Indeed, the melting models of Altherr et al. (2019) and Sanfilippo et al. (2019), consistently provide that the pipe basalts are produced from an amphibole-bearing garnet lherzolite at a degree of melting of 3%. Geobarometric and geothermometric data from xenoliths suggest that the present-day lithosphere under the Arabian rift shoulder is less than 80 km thick, whereas the crust has a normal thickness of about 35–40 km (McGuire and Bohannon, 1989). However, at the time of the formation of the volcanic pipes (Late Cretaceous–Early Eocene), before Red Sea rifting and continental rupturing, the lithosphere was thicker. Assuming a fertile lherzolite or a pyroxenite as source of the Marthoum basalts, the presence of garnets constrains a minimum pressure of 2.5–3.0 GPa where the parental melts of the pipes were generated, corresponding to a depth of ~70–90 km.

Further constraints on the diversity of mantle sources of Uwayrid lavas and pipe basalts are provided by their radiogenic isotopes. Basalts from volcanic pipes have lower $^{143}\text{Nd}/^{144}\text{Nd}$ and $^{176}\text{Hf}/^{177}\text{Hf}$ ratios, and higher $^{87}\text{Sr}/^{86}\text{Sr}$ and $^{206}\text{Pb}/^{204}\text{Pb}$ ratios that are more radiogenic, especially those of the most primitive and older pipes (site UH-10) (Figure 7). The slightly different isotopic composition of the two volcanic pipes was probably inherited from a heterogeneous mantle source because, as shown above, crustal contamination can be excluded as a cause of enrichment. In summary, the variations in major, trace and isotopic compositions of the Uwayrid and volcanic pipe basalts suggests parental melts produced by mixing of magma formed at different mantle depths and generated by a composite mantle source with enriched trace elements and initial isotopic heterogeneities. The most enriched end member at the base of the subcontinental lithosphere was probably sampled by the volcanic pipes.

Timing and Emplacement of the Marthoum Pipes

Only one radiometric age was available for the volcanic pipes; it yielded a Cretaceous age of 79 ± 3.7 Ma (Vaslet et al., 1994). The dated sample was from a large pipe (900 m in diameter) in the northern sector of the study area (Figure 2). However, the age obtained was considered incompatible with the known geology of the area (Vaslet et al., 1994), because some of the pipes contain rafts of fossiliferous Early Eocene sediments of the Mira formation. The new K-Ar age determinations, on the other

hand, confirm a Late Cretaceous–Early Eocene age for the emplacement of the Marthoum pipes suggesting that their injection within the thick continental crust was not a magmatic event confined to a short time interval, but lasted at least 30 Ma. This view is supported also by the RTP magnetic anomalies associated with the volcanic pipes indicating that their emplacement occurred through different normal and reverse epochs of the Earth's magnetic field (Figure 4).

Certainly, extensional stresses, prior to the rifting phase in the Red Sea, have affected a large area of northern-central Arabia, forming the system of horsts and grabens with NW-SE normal faults (the ribbon faults of Roobol and Stewart, 2019). The volcanic pipes are aligned precisely along this direction (Liddicoat, 1982; Vaslet et al., 1994). Although there are no time constraints determined for this stretching phase of the Arabian continental lithosphere, the angular discordance with respect to the underlying Late Cretaceous sequences (Aruma Formation) and early Eocene (Mira Formation) sedimentary formations, preserved within the Tabuk graben (Vaslet et al., 1994), lead one to suppose that they are syn-tectonic deposits suggesting an extensional phase during the time interval when the Marthoum pipes were emplaced. This extensional stress field has probably favoured the ascent of deep melts in isolated conduits which, meeting the water table in the Paleozoic sandstones, gave rise to the violent phreatomagmatic explosions that originated the Marthoum pipes. This is also suggested by the quenching history of their columnar basalts highlighted by the low-coercivity magnetic grain sizes (Figure 8F). The PSD grains (UnMix component₁) are formed by sudden cooling during the phreatomagmatic phase whereas the coarser MD grains (UnMix component₂) are formed by post-intrusion cooling. The proportion between the two components (0.8 vs. 0.198) indicates a clear predominance of rapid cooling on magnetic grain-size fragmentation (Figure 8F).

A HIMU-Like Source in the African-Arabian Lithosphere

Several authors pointed out that almost all alkaline lavas of the Arabian Plate have relatively low $^{143}\text{Nd}/^{144}\text{Nd}$, $^{143}\text{Hf}/^{144}\text{Hf}$ and $^{87}\text{Sr}/^{86}\text{Sr}$ isotopic ratios, and radiogenic $^{206}\text{Pb}/^{204}\text{Pb}$ ratio (Altherr et al., 1990; Stein and Hofmann, 1992; Bertrand et al., 2003; Shaw et al., 2003; Moufti et al., 2012; Rooney et al., 2014). These isotopic signatures indicate the involvement of a source with a high time-integrated $^{238}\text{U}/^{206}\text{Pb}$ ratio, for relatively low $^{87}\text{Rb}/^{86}\text{Sr}$, $^{143}\text{Sm}/^{144}\text{Nd}$ and $^{176}\text{Lu}/^{177}\text{Hf}$. These compositions point to a HIMU-like signature, similar to that of some OIBs (Zindler and Hart, 1986; Hofmann, 1997). This is further sustained by the local occurrence of mantle xenoliths having similar isotopic compositions (Baker et al., 1997). Altherr et al. (2019) questioned this idea suggesting that the compositions of the Arabian lava fields plot close to the “PREMA” (PREvalent MANTle) mantle component (Zindler and Hart, 1986), as defined in oceanic basalts. An important finding of our study is that the isotopic compositions of the sampled volcanic pipes plot out of the field of the Cenozoic Arabian alkaline volcanism, being by far more enriched in Nd-Hf-Sr and Pb isotopes than any lava ever reported in western Arabia

(Figure 7). Their compositions are distinct from typical “PREMA” signatures, being less radiogenic in Nd and Hf isotopes. The Marthoum volcanic pipes have an isotopic signature similar to that of the HIMU-like lava fields of eastern Africa, thus testifying to a “HIMU-like” end-member in the source of Arabian magmatism.

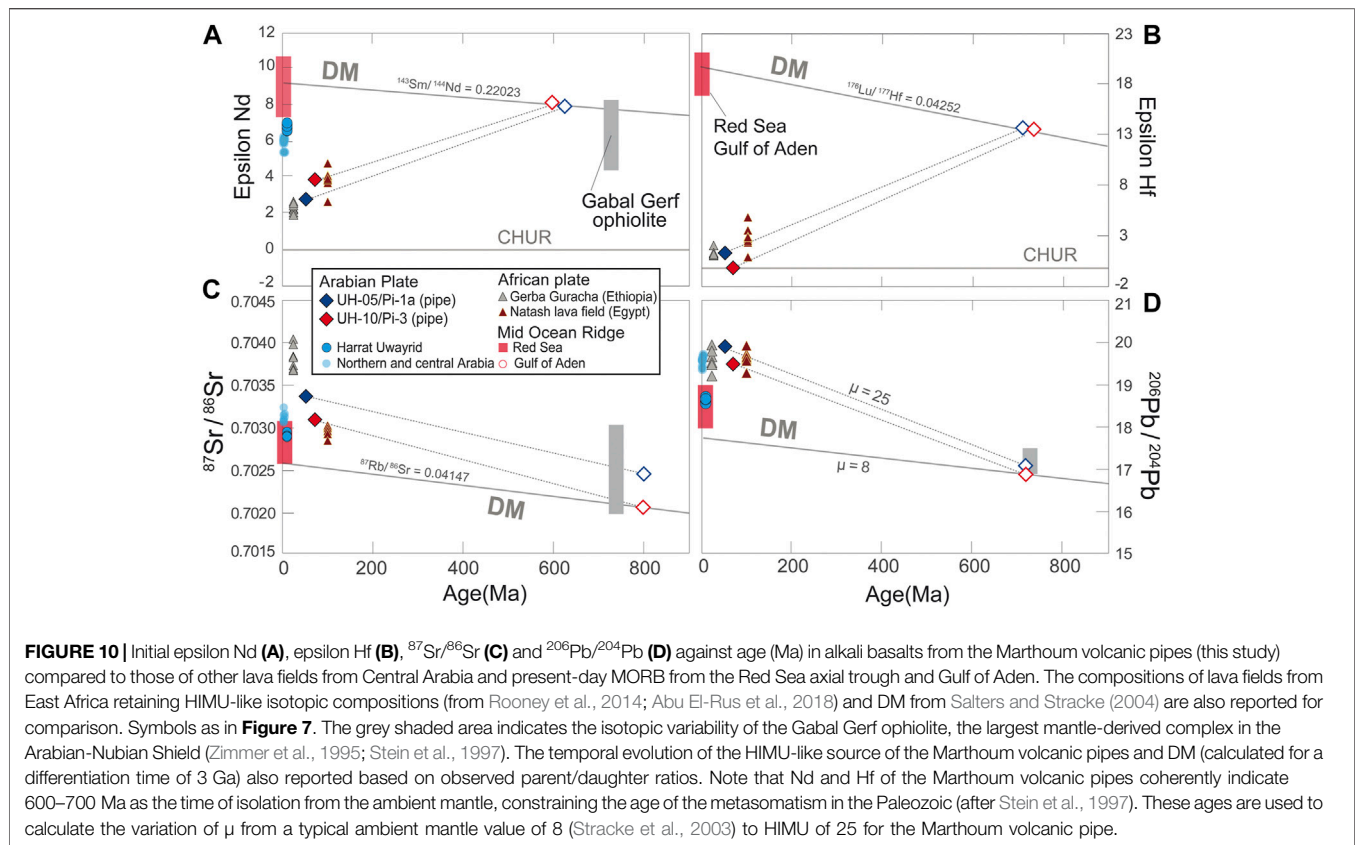
The origin of the HIMU-like component in the source of Cenozoic lavas of the African and Arabian Plates has been widely debated. Based on the areal distribution and type of volcanism along the Arabian Shield, Camp and Robool (1992) first proposed that the enriched material fueling Arabian volcanism derives from the northward channeling of the Afar plume along a N-S lithospheric channel. This model was further supported by paired geochemical and geophysical observations (Krienitz et al., 2009; Chang and Van der Lee, 2011; Duncan and Al-Amri, 2013; Duncan et al., 2016) suggesting a radial flow of material away from Afar channeled along zones of thinned lithosphere (Lim et al., 2020). Although material derived from the Afar plume may have influenced Arabian magmatism in the southern Red Sea region (Bertrand et al., 2003), Figure 7 shows that the isotopic compositions of most western Arabia lava fields lay on trends pointing towards an enriched source different from the Afar plume (Rooney et al., 2012), with a more enriched Nd and Hf isotope content and a less radiogenic Sr. K-Ar age determinations indicate that Marthoum pipes formed during the Late Cretaceous to the Early Eocene, thus predating the impingement of the Afar plume. We can now exclude any connection between the HIMU-like source of our samples with asthenospheric material derived from the Afar plume. Rather, the widespread distribution of the HIMU-like signature from Israel and Syria (Stein and Hoffman, 1992; Shaw et al., 2007), Saudi Arabia (Bertrand et al., 2003; Moufti et al., 2012; Altherr et al., 2019), eastern Africa (Rooney et al., 2014; Abu El-Rus et al., 2018) and, locally, in the Gulf of Aden MORB (Schilling et al., 1992) indicates that a HIMU-like composition fits the cratonic Arabian lithosphere.

Stein et al. (1997) proposed that a HIMU-like isotopic composition develops in the subcontinental lithosphere as a consequence of rock-melt and rock-fluid interactions in the mantle wedge above a subduction zone. Hydrous melt migration from the base of a mantle wedge enriches the supra-subduction depleted mantle of incompatible elements such as LILE, U, Th and REE, forming peridotites enriched in magmatic amphiboles. During the subsequent de-hydration due to the thickening of the lithosphere, the elements with higher mobility in fluids, such as Pb and Rb, are preferentially removed leaving a refertilized mantle with low Rb/Sr and high U/Pb ratios. This process can then produce fertile domains, or “metasomes,” accreted in the lower part of the cratonic lithosphere and may develop over time high Pb-isotopes with relatively low Sr (Bertrand et al., 2003; Shaw et al., 2003; Shaw et al., 2007; Moufti et al., 2012; Rooney et al., 2014). This process can be evaluated analyzing the isotopic evolution of the Afro-Arabian mantle based on the observed isotopic ratios of western Arabian volcanism. Mantle melting has little effects on elements with similar compatibility; hence we can assume that the Sm/Nd and

Lu/Hf ratios of alkaline lavas, formed by enriched metasomes, have values close to those of their sources (e.g., Pilet et al., 2008; Rooney et al., 2014). Given that the Proterozoic crust of the Arabian Shield is considered to derive directly from upper mantle melting (Stein and Goldstein, 1996; Stern and Johnson, 2010 and references therein), we can reasonably assume that the ambient mantle modified by the metasomatic event was an upper mantle, depleted in incompatible elements before being modified and accreted at the base of the subcontinental lithosphere. Based on this, the time when the metasomes were isolated from the ambient mantle approaches the time of the metasomatism. Therefore, we calculated Nd-Hf model ages using a DM composition from Salters and Stracke (2004). Both volcanic pipes give ages ranging between 650 and 750 Ma. These ages are similar to the $^{143}\text{Sm}/^{144}\text{Nd}$ and $^{176}\text{Lu}/^{177}\text{Hf}$ model ages obtained for the HIMU-like lava fields in eastern Africa (Rooney et al., 2014; Abu El-Rus et al., 2018) and support the hypothesis that the metasomatic event is related to the Panafrican orogeny (Stein et al., 1997).

The Nd-Hf-Sr-Pb isotopic evolution of the HIMU-like source is illustrated in Figure 10, along with the compositions of magmatism in the region. The age-corrected isotopic composition of the HIMU-like lavas from Egypt (~90 Ma; Abu El-Rus et al., 2019) and Ethiopia (24 Ma; Rooney et al., 2014) plot along the evolutionary line defined by the Marthoum pipes, with the only exception of the higher $^{87}\text{Sr}/^{86}\text{Sr}$ of the Gerba Guracha basalts. Here, the higher $^{87}\text{Sr}/^{86}\text{Sr}$ isotopes can be possibly related to the influence of the Afar Plume. Taken together, our calculation shows that the Paleozoic metasomatic process changed the parent/daughter ratios of the DM peridotites (calculated for a differentiation time of 3 Ga; Salters and Stracke, 2004), leading to an increase of $^{238}\text{U}/^{206}\text{Pb}$ ($u = 8$ to $u = 25$), and decreases of $^{143}\text{Sm}/^{144}\text{Nd}$ (0.220–0.135) and $^{176}\text{Lu}/^{177}\text{Hf}$ (0.042–0.005), along with small variations of $^{87}\text{Rb}/^{86}\text{Sr}$ ratios (0.041–0.084). These variations are in agreement with the two-stages process of magmatic metasomatism from hydrous-melts, followed by dehydration at the base of the lithosphere as proposed by Stein et al. (1997). Alternatively, Abu El-Rus et al. (2019) proposed that the ancient refertilization was driven by carbonatite melts, in part following suggestions of Weiss et al. (2016) for the origin of the oceanic HIMU. They pointed out that Hf-Nd-Sr-Pb isotopes and trace-element patterns support a genetic relationship between HIMU lavas and metasomatized carbonated peridotite sources in the subcontinental lithospheric mantle (SCLM) (Tilton and Bell, 1994; Bizimis et al., 2003). During the metasomatic event, the interaction of a depleted mantle with a deep carbonatite melt can produce fertile lithologies having high U-Th/Pb, low Sm-Nd, Lu-Hf and Rb-Sr ratios, developing an HIMU character over time. The very low Al_2O_3 contents (Figure 5C), the high Nb/Zr-Hf ratios, and the depletions in alkali (Rb, Cs, K) compared to other highly incompatible elements (Ba, Th, U, La) of the Marthoum pipes are consistent with this scenario (see Abu El-Rus et al., 2019).

The chemical modifications imposed by migrating melt during a refertilization process are dependent on the different incompatibility between the parent/daughter elements. In general, percolating melts, generated by an asthenospheric



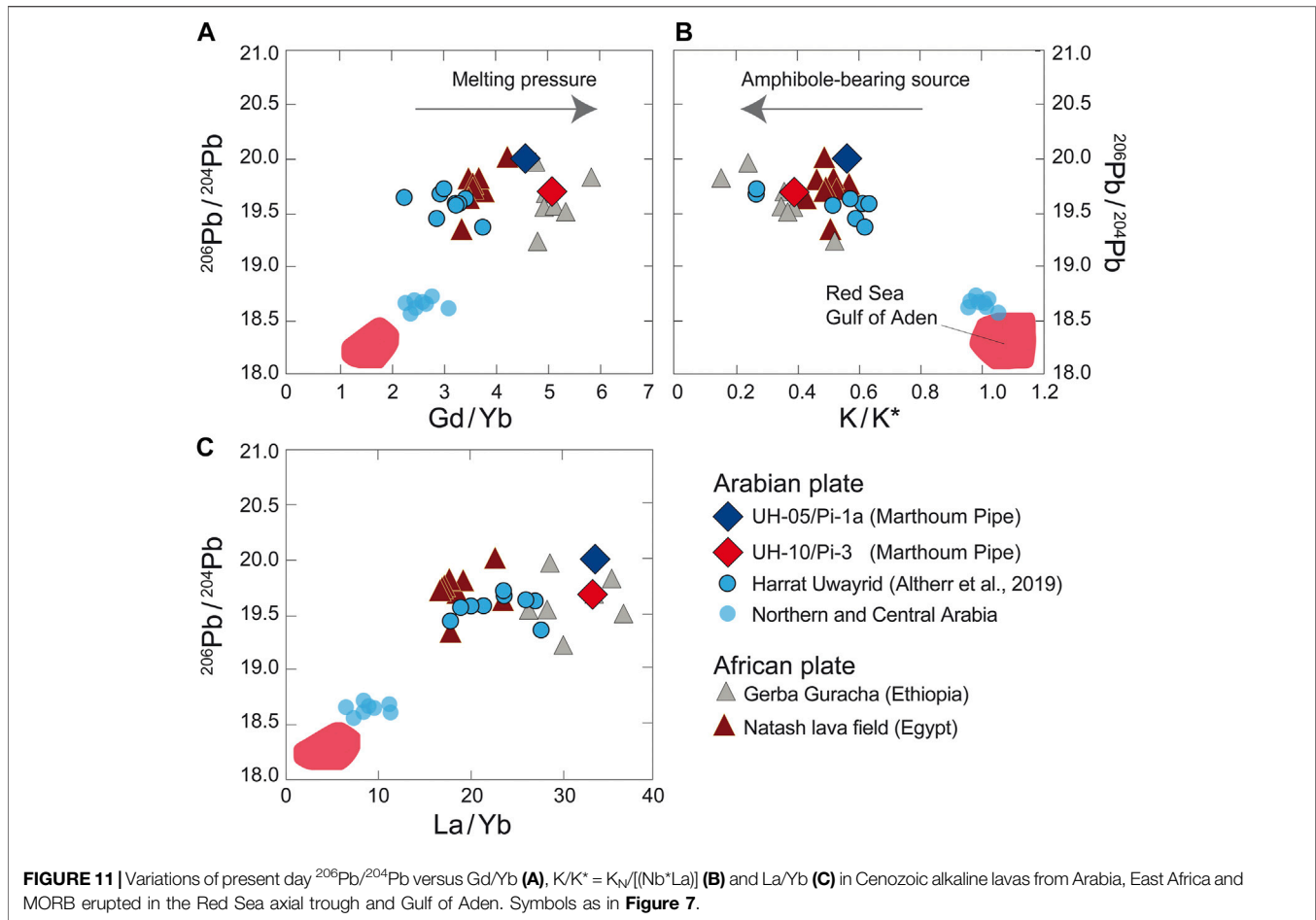
source, have higher (Th)U/Pb, Rb/Sr, and lower Sm/Nd and Lu/Hf ratios than the residual mantle, and are thereby able to produce enriched isotopic signatures over time (see Stracke, 2012). Due to the much greater difference in incompatibility between Rb and Sr compared to Sm and Nd or Lu and Hf, ancient melt-rock reactions result in a refertilized mantle with high Sr isotopes for relatively low Nd and Hf isotopic ratios, although the $^{87}\text{Rb}/^{86}\text{Sr}$ ratio of the initial melt is low. Highly radiogenic Sr signatures are not seen in the Marthoum pipes (Figure 7), which plot well below oceanic basalts in the Nd/Hf vs. Sr isotopic space. The low initial $^{87}\text{Rb}/^{86}\text{Sr}$ ratio coupled with low $^{143}\text{Sm}/^{144}\text{Nd}$ and $^{176}\text{Lu}/^{177}\text{Hf}$ are therefore better explained by a de-hydration process of a mantle source previously enriched in incompatible trace elements.

Another explanation could be that the HIMU-like signature derives from material placed at the base of the lithosphere from a mantle plume. Based on recurring eruptions of alkali basalt with an isotopically enriched signature in Israel since ~200 Ma, Stein and Hoffman (1992) proposed that deep-stored material was accreted at the base of the lithosphere in the Jurassic by a rising mantle plume. A “fossilized” plume head, partially homogenized with the ambient mantle, should therefore be located in the lowermost portion of the cratonic lithosphere in northern Arabia since the Early Jurassic, remobilized and melted during the Red Sea rifting and related thinning of the lithosphere. However, Israel basalt compositions are much more radiogenic in Nd and Hf, and slightly less radiogenic in Sr than those of the Marthoum pipes (Stein and Hoffman, 1992). If a

homogenized plume-head exists below Israel, the Marthoum pipes formed from an enriched portion, less homogenized with the ambient mantle. The Nd and Hf model ages of the Marthoum pipes, and of the others Arabian lava fields with HIMU-like isotopic components in their mantle source as in those of eastern Africa, coherently suggest that the chemical differentiation of this enriched source from the ambient depleted mantle occurred ~700–800 Ma. Furthermore, structural analysis based on the sedimentary sequences of the Arabian platform indicates a persistent differentiation since 550 Ma of the geological histories of the uplifting Arabian Shield and the subsiding Arabian platform, questioning the emplacement of a mantle plume during the Jurassic (Stern and Johnson, 2010). Thus, although the existence of a fossilized plume distinct from the Afar and centered in the northern Arabia cannot be ruled out, our preferred hypothesis for the origin of the HIMU-like character in the Arabian-African alkaline volcanism is that it derives from a lithosphere enriched by an ancient process of deep refertilization and de-hydration of the mantle wedge during the Panafrican orogeny.

Widespread HIMU-Like Character in the Arabian Cenozoic Volcanism

Next we will show that the enriched signature documented in the Marthoum pipes is ubiquitous and widespread in the lower part of the Arabian lithosphere. Figure 11 shows the co-variations of Gd/Yb and La/Yb ratios, and of the K anomaly with the Pb and Sr



isotopes of western Arabian basalts (Bertrand et al., 2003; Moufti et al., 2012), of Red Sea and Gulf of Aden MORBs (Altherr et al., 1988; Eissen et al., 1989; Volker et al., 1993; Volker et al., 1997) and of the two HIMU-like African lava fields (Rooney et al., 2014; Abu El-Rus et al., 2018). Regardless of their age and geographic location, the western Arabia alkali-basalts lie on binary mixing lines connecting asthenospheric (DM) components with MORB composition, and the enriched component residing in Marthoum pipes and in HIMU-like East Africa lava fields. These correlations suggest that melt from this HIMU-like isotopic enriched source is generated preferentially at depth, and is variably mixed with melt from a more depleted – typically asthenospheric – upper mantle. The progressive deepening of the K-anomaly and overall increase of La/Yb and La/Sm ratios towards the more enriched isotopic compositions (i.e., high Sr and Pb, low Nd and Hf isotopic ratios) suggest that the enriched end-member may be represented by an amphibole- and garnet-bearing lithospheric mantle (Rooney et al., 2014). Another consequence of the correlations in Figure 11 is that the enriched character appears to gradually fade as the mean depth of melting decreases and the degree of melting

increases. This is counterintuitive, as the contribution of the enriched lithosphere would be expected to be stronger at shallower depths, and then reduced by mixing with melts from a depleted asthenosphere beneath the continental roots. We therefore propose that the enriched portions of the lithosphere are thermally eroded and physically removed during progressive thinning of the lithospheric lid by regional extension and mantle upwelling. Under these conditions, the fertile geochemical components are preferentially melted at depth and at low degrees of melting. As the extension proceeds, the amount of melt from the enriched source progressively decreases and its contribution is easily concealed by mixing with melts produced by a depleted asthenosphere. Consequently, the enriched character would be better preserved in the pre-rift volcanism generated beneath a thick continental lithosphere: a constraint fully satisfied by the Marthoum pipes. The almost complete absence of such enriched compositions in the central Red Sea MORB (Altherr et al., 1992) and in most of the Gulf of Aden (Schilling et al., 1992), where the asthenospheric component is dominant, further supports this hypothesis and indicates that this enriched source was almost completely removed during thermal erosion of the

subcontinental lithospheric mantle at the onset of seafloor spreading (Bertrand et al., 2003).

CONCLUSION

An extensional phase prior to Red Sea rifting during Late Cretaceous-Early Eocene times induced shearing and stretching of the thick continental lithosphere of the Arabian Shield. The limited and localized lithospheric thinning induced a minor thermobaric perturbation in the continental mantle, sufficient to allow the fusion of a low solidus component of the mantle source at the cratonic roots. Extensional faults favoured the ascent through the entire continental lithosphere of these deep melts, which, meeting at shallow levels the water table in the Paleozoic sandstones, gave rise to the violent phreatomagmatic explosions that led to the Marthoum pipes. The erupted lavas have Sr-Pb-Nd-Hf isotopic ratios far from the Cenozoic Arabian alkaline volcanism field, being much more enriched in Nd-Hf and Pb isotopes than any Arabian Plate lava. Basalt geochemistry indicates that these volcanic eruptions were due to melts generated by low-degree partial melting of an enriched lithospheric source with composition similar to the HIMU-like enriched isotopic component from the East African Rift and considered to represent the lowermost lithospheric mantle of the Arabian-Nubian Shield. In fact, the pervasive metasomatism of the lithospheric mantle during the Neoproterozoic generated widespread, easily fusible amphibole-rich metasomes within the shield juvenile lithosphere. The generated melt mixed with melt derived from a depleted asthenosphere, produces the observed HIMU-like character of the Cenozoic Arabian alkaline volcanism. Although apparently hidden, this enriched lithospheric component is therefore ubiquitous and widespread in the cratonic roots of the African and Arabian lithospheric mantle.

DATA AVAILABILITY STATEMENT

The original contributions presented in the study are included in the article/**Supplementary Material**, further inquiries can be directed to the corresponding author.

REFERENCES

- Abu El-Rus, M. A., Chazot, G., Vannucci, R., and Paquette, J.-L. (2018). Tracing the HIMU Component within Pan-African Lithosphere beneath Northeast Africa: Evidence from Late Cretaceous Natash Alkaline Volcanics, Egypt. *Lithos* 300-301, 136–153. doi:10.1016/j.lithos.2017.11.037
- Abu El-Rus, M. A., Paquette, J.-L., Chazot, G., and Vannucci, R. (2019). Bimodal Zircon Ages from Natash Volcanics (Southeast Egypt) and the Link between Eruption Mechanisms and Late Cretaceous Tectonics. *Arab. J. Geosci.* 12, 291. doi:10.1007/s12517-019-4457-2
- Abu El-Rus, M. M. A., and Rooney, T. O. (2017). Insights into the Lithosphere to Asthenosphere Melting Transition in Northeast Africa: Evidence from the Tertiary Volcanism in Middle Egypt. *Chem. Geology.* 455, 282–303. doi:10.1016/j.chemgeo.2016.10.005

AUTHOR CONTRIBUTIONS

AS, NR, LV, and ML developed the ideas and the methods for this study. AS and ML wrote jointly the paper with contributions from CS, IS, NR, and LV. AS, NR, LV, NW, AO, and ML carried out fieldwork in the study area. AS and CS did geochemistry work, IS performed the aeromagnetic data analysis and LV conducted laboratory work for magnetic properties and paleomagnetism. All the authors discussed extensively the results and the interpretations.

FUNDING

The work was supported by the SGS and the Italian Consiglio Nazionale Ricerche. The research was sponsored by the PRIN2017 Programme (PRIN_2017KY5ZX8).

ACKNOWLEDGMENTS

This work is the result of a joint effort of the Saudi Geological Survey (SGS), and the Istituto di Scienze Marine, CNR of Bologna (ISMAR-CNR). We particularly thank Captain P. Dimala and helicopter assistants Abdulhadi and A. Al-Harbi for their collaboration during the fieldwork. We thank Z. A. Nawab, former SGS President and A. M. Alattas, former SGS Assistant President for Technical Affairs. We would also like to extend our thanks to the Assistant President, Technical Affairs, Saleh A. Sefry for his cooperation and support in publishing this research. Colleagues at the Center for Marine Geology (CMG-SGS) are also thanked for their participation and assistance in the numerous field expeditions. We thank A. Winkler for measuring the FORC diagram.

SUPPLEMENTARY MATERIAL

The Supplementary Material for this article can be found online at: <https://www.frontiersin.org/articles/10.3389/feart.2021.699460/full#supplementary-material>

- Altherr, R., Henjes-Kunst, F., and Baumann, A. (1990). Asthenosphere versus Lithosphere as Possible Sources for Basaltic Magmas Erupted during Formation of the Red Sea: Constraints from Sr, Pb and Nd Isotopes. *Earth Planet. Sci. Lett.* 96, 269–286. doi:10.1016/0012-821X(90)90007-K
- Altherr, R., Henjes-Kunst, F., Puchelt, H., and Baumann, A. (1988). Volcanic Activity in the Red Sea Axial Trough - Evidence for a Large Mantle Diapir? *Tectonophysics* 150, 121–133. doi:10.1016/0040-1951(88)90298-3
- Altherr, R., Mertz-Kraus, R., Volker, F., Kreuzer, H., Henjes-Kunst, F., and Lange, U. (2019). Geodynamic Setting of Upper Miocene to Quaternary Alkaline Basalts from Harrat Al 'Uwayrid (NW Saudi Arabia): Constraints from K Ar Dating, Chemical and Sr-Nd-Pb Isotope Compositions, and Petrological Modeling. *Lithos* 330-331, 120–138. doi:10.1016/j.lithos.2019.02.007
- Baker, J. A., Menzies, M. A., Thirlwall, M. F., and MacPherson, C. G. (1997). Petrogenesis of Quaternary Intraplate Volcanism, Sana'a, Yemen: Implications

- for Plume-Lithosphere Interaction and Polybaric Melt Hybridization. *J. Petrol.* 38, 1359–1390. doi:10.1093/ptetro/38.10.1359
- Baker, J. A., Thirlwall, M. F., and Menzies, M. A. (1996). Sr-Nd-Pb Isotopic and Trace Element Evidence for Crustal Contamination of Plume-Derived Flood Basalts: Oligocene Flood Volcanism in Western Yemen. *Geochimica et Cosmochimica Acta* 60, 2559–2581. doi:10.1016/0016-7037(96)00105-6
- Barberi, F., and Varet, J. (1977). Volcanism of Afar: Small Scale Plate Tectonics Implications. *Bull. Geol. Soc. Am.* 88, 1251–1266. doi:10.1130/0016-7606(1977)88<1251:VOASPT>2.0.CO;2
- Belshaw, N. S., Freedman, P. A., O’Nions, R. K., Frank, M., and Guo, Y. (1998). A New Variable Dispersion Double-Focusing Plasma Mass Spectrometer with Performance Illustrated for Pb Isotopes. *Int. J. Mass Spectrom.* 181, 51–58. doi:10.1016/S1387-3806(98)14150-7
- Bertrand, H., Chazot, G., Blichert-Toft, J., and Thoral, S. (2003). Implications of Widespread High- μ Volcanism on the Arabian Plate for Afar Mantle Plume and Lithosphere Composition. *Chem. Geology*. 198, 47–61. doi:10.1016/S0009-2541(02)00418-7
- Bizimis, M., Salters, V. J. M., and Dawson, J. B. (2003). The Brevity of Carbonatite Sources in the Mantle: Evidence from Hf Isotopes. *Contrib. Mineralogy Petrol.* 145, 281–300. doi:10.1007/s00410-003-0452-3
- Blank, H. R. (1977). Aeromagnetic and Geological Study of Tertiary Dikes and Related Structures on the Arabian Margin of the Red Sea. *MINER. RESOURCES BULL.; Sau; DA* 22, G1–G18.
- Blichert-Toft, J., and Albarède, F. (1997). The Lu-Hf Isotope Geochemistry of Chondrites and the Evolution of the Mantle-Crust System. *Earth Planet. Sci. Lett.* 148, 243–258. doi:10.1016/S0012-821X(97)00040-X
- Bohannon, R. G., Naeser, C. W., Schmidt, D. L., and Zimmermann, R. A. (1989). The Timing of Uplift, Volcanism, and Rifting Peripheral to the Red Sea: A Case for Passive Rifting? *J. Geophys. Res.* 94, 1683–1701. doi:10.1029/JB094iB02p01683
- Bosworth, W., Huchon, P., and McClay, K. (2005). The Red Sea and Gulf of Aden Basins. *J. Afr. Earth Sci.* 43, 334–378. doi:10.1016/j.jafrearsci.2005.07.020
- Bosworth, W., and Stockli, D. F. (2016). Early Magmatism in the Greater Red Sea Rift: Timing and Significance. *Can. J. Earth Sci.* 53, 1158–1176. doi:10.1139/cjes-2016-0019
- Brown, G. F., Schmidt, D. L., and Huffman, A. C. (1989). *Geology of the Arabian Peninsula: Shield Area of Western Saudi Arabia*. Reston, Virginia: United States Geological Survey, Professional paper 560-A, 188.
- Camp, V. E., and Roobol, M. J. (1992). Upwelling Asthenosphere beneath Western Arabia and its Regional Implications. *J. Geophys. Res.* 97, 15255–15271. doi:10.1029/92JB00943
- Chadwick, W. W., and Embley, R. W. (1998). Graben Formation Associated with Recent dike Intrusions and Volcanic Eruptions on the Mid-ocean ridge. *J. Geophys. Res.* 103, 9807–9825. doi:10.1029/97JB02485
- Chang, S.-J., and Van der Lee, S. (2011). Mantle Plumes and Associated Flow beneath Arabia and East Africa. *Earth Planet. Sci. Lett.* 302, 448–454. doi:10.1016/j.epsl.2010.12.050
- Chazot, G., and Bertrand, H. (1993). Mantle Sources and Magma-continental Crust Interactions during Early Red Sea-Gulf of Aden Rifting in Southern Yemen: Elemental and Sr, Nd, Pb Isotope Evidence. *J. Geophys. Res.* 98, 1819–1835. doi:10.1029/92JB02314
- Coleman, R. G. (1993). *Geologic Evolution of the Red Sea Oxford Monographs on Geology and Geophysics*. New York: Oxford University Press, 186.
- Coleman, R. G., Gregory, R. T., and Brown, G. F. (1983). “Cenozoic Volcanic Rocks of Saudi Arabia.”. Open File Report USGS-OF93 (Reston, Virginia: Saudi Arabian Deputy Minister of Mineral Resources), 82.
- Coleman, R. G., and McGuire, A. V. (1988). Magma Systems Related to the Red Sea Opening. *Tectonophysics* 150, 77–100. doi:10.1016/0040-1951(88)90296-X
- Creaser, R. A., Erdmer, P., Stevens, R. A., and Grant, S. L. (1997). Tectonic Affinity of Nisutlin and Anvil Assemblage Strata from the Teslin Tectonic Zone, Northern Canadian Cordillera: Constraints from Neodymium Isotope and Geochemical Evidence. *Tectonics* 16, 107–121. doi:10.1029/96TC03317
- Creaser, R. A., Grütter, H., Carlson, J., and Crawford, B. (2004). Macrocrystal Phlogopite Rb-Sr Dates for the Ekati Property Kimberlites, Slave Province, Canada: Evidence for Multiple Intrusive Episodes in the Paleocene and Eocene. *Lithos* 76, 399–414. doi:10.1016/j.lithos.2004.03.039
- Dalou, C., Koga, K. T., Hammouda, T., and Poitrasson, F. (2009). Trace Element Partitioning between Carbonatitic Melts and Mantle Transition Zone Minerals: Implications for the Source of Carbonatites. *Geochimica et Cosmochimica Acta* 73, 239–255. doi:10.1016/j.gca.2008.09.020
- Deniel, C., Vidal, P., Coulon, C., Vellutini, P.-J., and Piguet, P. (1994). Temporal Evolution of Mantle Sources during continental Rifting: The Volcanism of Djibouti (Afar). *J. Geophys. Res.* 99, 2853–2869. doi:10.1029/93JB02576
- Duncan, R. A., and Al-Amri, A. M. (2013). Timing and Composition of Volcanic Activity at Harrat Lunayyir, Western Saudi Arabia. *J. Volcanology Geothermal Res.* 260, 103–116. doi:10.1016/j.jvolgeores.2013.05.006
- Duncan, R. A., Kent, A. J. R., Thomber, C. R., Schlieder, T. D., and Al-Amri, A. M. (2016). Timing and Composition of continental Volcanism at Harrat Hutaymah, Western Saudi Arabia. *J. Volcanology Geothermal Res.* 313, 1–14. doi:10.1016/j.jvolgeores.2016.01.010
- Ebinger, C. J., Deino, A. L., Tesha, A. L., Becker, T., and Ring, U. (1993). Tectonic Controls on Rift basin Morphology: Evolution of the Northern Malawi (Nyasa) Rift. *J. Geophys. Res.* 98, 17821–17836. doi:10.1029/93JB01392
- Eissen, J.-P., Juteau, T., Joron, J.-L., Dupre, B., Humler, E., and Al’Mukhamedov, A. (1989). Petrology and Geochemistry of Basalts from the Red Sea Axial Rift at 18 North. *J. Petrol.* 30, 791–839. doi:10.1093/ptetrology/30.4.791
- Fisher, R. (1953). Dispersion on a Sphere. *Proc. R. Soc. A: Math. Phys. Eng. Sci.* 217, 295–305. doi:10.1098/rspa.1953.0064
- Gale, A., Dalton, C. A., Langmuir, C. H., Su, Y., and Schilling, J.-G. (2013). The Mean Composition of Ocean ridge Basalts. *Geochem. Geophys. Geosyst.* 14, 489–518. doi:10.1029/2012GC004334
- Gale, A., Escrig, S., Gier, E. J., Langmuir, C. H., and Goldstein, S. L. (2011). Enriched Basalts at Segment Centers: The Lucky Strike (37°17’N) and Menez Gwen (37°50’N) Segments of the Mid-Atlantic Ridge. *Geochem. Geophys. Geosyst.* 12, a-n. doi:10.1029/2010GC003446
- Green, T. H., Blundy, J. D., Adam, J., and Yaxley, G. M. (2000). SIMS Determination of Trace Element Partition Coefficients between Garnet, Clinopyroxene and Hydrous Basaltic Liquids at 2–7.5 GPa and 1080–1200°C. *Lithos* 53, 165–187. doi:10.1016/S0024-4937(00)00023-2
- Grove, T. L., Kinzler, R. J., and Bryan, W. B. (1992). “Fractionation of Mid-ocean Ridge Basalt (MORB).” Mantle Flow and Melt Generation At Mid-ocean Ridges. *Am. Geophys. Union Geophysical Monograph*. Editors J. P. Morgan, D. K. Blackman, and J. M. Sinton, 71, 281–310. doi:10.1029/GM071p0281
- Haase, K. M., Mühe, R., and Stoffers, P. (2000). Magmatism during Extension of the Lithosphere: Geochemical Constraints from Lavas of the Shaban Deep, Northern Red Sea. *Chem. Geology*. 166, 225–239. doi:10.1016/S0009-2541(99)00221-1
- Harrison, L. N., Weis, D., and Garcia, M. O. (2017). The Link between Hawaiian Mantle Plume Composition, Magmatic Flux, and Deep Mantle Geodynamics, and Deep Mantle Geodynamics. *Earth Planet. Sci. Lett.* 463, 298–309. doi:10.1016/j.epsl.2017.01.027
- Hatcher, R. D., Zietz, I., Regan, R. D., and Abu-Ajamieh, M. (1981). Sinistral Strike Slip Motion on the Dead Sea Rift: Confirmation from New Magnetic Data. *Geology* 9, 458–462. doi:10.1130/0091-7613(1981)9<458:SSMOTD>2.0.CO;2
- Hofmann, A. W., and Farnetani, C. G. (2013). Two Views of Hawaiian Plume Structure. *Geochem. Geophys. Geosyst.* 14, 5308–5322. doi:10.1002/2013GC004942
- Hofmann, A. W., Jochum, K. P., Seufert, M., and White, W. M. (1986). Nb and Pb in Oceanic Basalts: New Constraints on Mantle Evolution. *Earth Planet. Sci. Lett.* 79, 33–45. doi:10.1016/0012-821X(86)90038-5
- Hofmann, A. W. (1997). Mantle Geochemistry: the Message from Oceanic Volcanism. *Nature* 385, 219–229. doi:10.1038/385219a0
- Holmden, C., Creaser, R. A., and Muehlenbachs, K. (1997). Paleosalinities in Ancient Brackish Water Systems Determined by 87Sr/86Sr Ratios in Carbonate Fossils: A Case Study from the Western Canada Sedimentary basin. *Geochimica et Cosmochimica Acta* 61, 2105–2118. doi:10.1016/S0016-7037(97)00073-2
- Ibrahim, K. M., Tarawneh, K., and Rabba’, I. (2003). Phases of Activity and Geochemistry of Basaltic dike Systems in Northeast Jordan Parallel to the Red Sea. *J. Asian Earth Sci.* 21, 467–472. doi:10.1016/S1367-9120(02)00075-5
- Johnson, P. R., and Vranas, G. J. (1992). “Qualitative Interpretation of Aeromagnetic Data for the Arabian Shield.”. Open-File Report USGS-OF-92-1, 34 p., 2 plates (Reston, Virginia Saudi Arabian Directorate General of Mineral Resources).
- Kaliwoda, M., Altherr, R., and Meyer, H.-P. (2007). Composition and thermal Evolution of the Lithospheric Mantle beneath the Harrat Uwayrid, Eastern Flank of the Red Sea Rift (Saudi Arabia) flank of the Red Sea Rift (Saudi Arabia). *Lithos* 99, 105–120. doi:10.1016/j.lithos.2007.06.013
- Khon, B. P., Lang, B., and Steinitz, G. (1993). ⁴⁰Ar/³⁹Ar Dating of the Atlit-1 Volcanic Sequence, Northern Israel. *Isr. J. Earth-Sci.* 42, 17–28.

- Kirschvink, J. L. (1980). The Least-Squares Line and Plane and the Analysis of Palaeomagnetic Data. *Geophys. J. Int.* 62, 699–718. doi:10.1111/j.1365-246X.1980.tb02601.x
- Krienitz, M.-S., Haase, K. M., Mezger, K., van den Bogaard, P., Thiemann, V., and Shaikh-Mashail, M. A. (2009). Tectonic Events, continental Intraplate Volcanism, and Mantle Plume Activity in Northern Arabia: Constraints from Geochemistry and Ar-Ar Dating of Syrian Lavas. *Geochem. Geophys. Geosyst.* 10, a–n. doi:10.1029/2008GC002254
- Lambart, S., Koornneef, J. M., Millet, M.-A., Davies, G. R., Cook, M., and Lissenberg, C. J. (2019). Highly Heterogeneous Depleted Mantle Recorded in the Lower Oceanic Crust. *Nat. Geosci.* 12, 482–486. doi:10.1038/s41561-019-0368-9
- Lang, B., and Steinitz, G. (1989). K-ar Dating of Mesozoic Magmatic Rocks in Israel: A Review. *Isr. J. Earth Sci.* 38, 89–103.
- Le Maitre, R. W., Streckeisen, A., Zanettin, B., Le Bas, M. J., Bonin, B., Bateman, P., et al. (2002). *Igneous Rocks: A Classification and Glossary of Terms, Recommendations of the International Union of Geological Sciences, Subcommission of the Systematics of Igneous Rocks*. Cambridge: Cambridge University Press, 236.
- Liddicoat, W. K. (1982). “Cenozoic Volcanic Pipes in the Marthoum Area (27/37D).” Open-File Report DGM-R-OF-03-11 (Jeddah: Saudi Arabian Deputy Ministry for Mineral Resources), 47.
- Ligi, M., Bonatti, E., Bortoluzzi, G., Cipriani, A., Cocchi, L., Caratori Tontini, F., et al. (2012). Birth of an Ocean in the Red Sea: Initial Pangs. *Geochem. Geophys. Geosyst.* 13, a–n. doi:10.1029/2012GC004155
- Ligi, M., Bonatti, E., Bosworth, W., Cai, Y., Cipriani, A., Palmiotto, C., et al. (2018). Birth of an Ocean in the Red Sea: Oceanic-type Basaltic Melt Intrusions Precede continental Rupture. *Gondwana Res.* 54, 150–160. doi:10.1016/j.gr.2017.11.002
- Ligi, M., Bonatti, E., and Rasul, N. M. A. (2015). “Seafloor Spreading Initiation: Geophysical and Geochemical Constraints from the Thetis and Nereus Deeps, Central Red Sea,” in *The Red Sea: The Formation, Morphology, Oceanography and Environment of a Young Ocean Basin*. Editors N. M. A. Rasul, and I. C. F. Stewart (Berlin, Heidelberg: Springer-Verlag), 79–98. doi:10.1007/978-3-662-45201-1_4
- Lim, J. A., Chang, S. J., Mai, P. M., and Zahran, H. (2020). Asthenospheric Flow of Plume Material beneath Arabia Inferred from S Wave Traveltime Tomography. *J. Geophys. Res. Solid Earth* 125, e2020JB019668. doi:10.1029/2020JB019668
- Mackenzie, G. D., Thybo, H., and Maguire, P. K. H. (2005). Crustal Velocity Structure across the Main Ethiopian Rift: Results from Two-Dimensional Wide-Angle Seismic Modelling. *Geophys. J. Int.* 162, 994–1006. doi:10.1111/j.1365-246X.2005.02710.x
- Maxbauer, D. P., Feinberg, J. M., and Fox, D. L. (2016). MAX UnMix: A Web Application for Unmixing Magnetic Coercivity Distributions. *Comput. Geosciences* 95, 140–145. doi:10.1016/j.cageo.2016.07.009
- McGuire, A. V., and Bohannon, R. G. (1989). Timing of Mantle Upwelling: Evidence for a Passive Origin for the Red Sea Rift. *J. Geophys. Res.* 94, 1677–1682. doi:10.1029/JB094iB02p01677
- McKenzie, D. (1986). Geophysics: Mantle Mixing Still a Mystery. *Nature* 323, 297. doi:10.1038/323297a0
- Moufti, M. R., Moghazi, A. M., and Ali, K. A. (2013). 40Ar/39Ar Geochronology of the Neogene-Quaternary Harrat Al-Madinah Intercontinental Volcanic Field, Saudi Arabia: Implications for Duration and Migration of Volcanic Activity. *J. Asian Earth Sci.* 62, 253–268. doi:10.1016/j.jseas.2012.09.027
- Moufti, M. R., Moghazi, A. M., and Ali, K. A. (2012). Geochemistry and Sr-Nd-Pb Isotopic Composition of the Harrat Al-Madinah Volcanic Field, Saudi Arabia. *Gondwana Res.* 21, 670–689. doi:10.1016/j.gr.2011.06.003
- Niu, Y., and Batiza, R. (1997). Trace Element Evidence from Seamounts for Recycled Oceanic Crust in the Eastern Pacific Mantle. *Earth Planet. Sci. Lett.* 148, 471–483. doi:10.1016/S0012-821X(97)00048-4
- Ogg, J. G. (2012). “Geomagnetic Polarity Time Scale,” in *The Geologic Time Scale 2012*. Editors F. M. Gradstein, J. G. Ogg, M. Schmitz, and G. Ogg (Elsevier), 85–113. doi:10.1016/B978-0-444-59425-9.00005-6
- Pallister, J. S. (1987). Magmatic History of Red Sea Rifting: Perspective from the central Saudi Arabian Coastal plain. *Geol. Soc. Am. Bull.* 98, 400–417. doi:10.1130/00167606(1987)98<400:MHORSR>2.0.CO;2
- Phoenix Corporation (1985). “The Interpretation of an Aeromagnetic Survey of the Cover Rocks Region, Kingdom of Saudi Arabia,”. unnumbered report (Jeddah: Saudi Arabian Deputy Ministry for Mineral Resources, DMMR).
- Pilet, S., Baker, M. B., and Stolper, E. M. (2008). Metasomatized Lithosphere and the Origin of Alkaline Lavas. *Science* 320, 916–919. doi:10.1126/science.1156563
- Presnall, D. C., Dixon, S. A., Dixon, J. R., O'Donnell, T. H., Brenner, N. L., Schrock, R. L., et al. (1978). Liquidus Phase Relations on the Join Diopside-Forsterite-Anorthite from 1 Atm to 20 Kbar: Their Bearing on the Generation and Crystallization of Basaltic Magma. *Contr. Mineral. Petrol.* 66, 203–220. doi:10.1007/BF0115029610.1007/bf00372159
- Roberts, A. P., Pike, C. R., and Verosub, K. L. (2000). First-order Reversal Curve Diagrams: A New Tool for Characterizing the Magnetic Properties of Natural Samples. *J. Geophys. Res.* 105, 28461–28475. doi:10.1029/2000JB900326
- Roobol, M. J., and Stewart, I. C. F. (2019). “Cenozoic Faults and Seismicity in Northwest Saudi Arabia and the Gulf of Aqaba Region,” in *Geological Setting, Palaeoenvironment and Archaeology of the Red Sea*. Editors N. M. A. Rasul and I. C. F. Stewart (Cham, Switzerland: Springer Earth System Sciences, Springer Nature), 275–305. doi:10.1007/978-3-319-99408-6_13
- Rooney, T. O., Bastow, I. D., and Keir, D. (2011). Insights into Extensional Processes during Magma Assisted Rifting: Evidence from Aligned Scoria Cones. *J. Volcanology Geothermal Res.* 201, 83–96. doi:10.1016/j.jvolgeores.2010.07.019
- Rooney, T. O., Hanan, B. B., Graham, D. W., Furman, T., Blichert-Toft, J., and Schilling, J.-G. (2012). Upper Mantle Pollution during Afar Plume-Continental Rift Interaction. *J. Petrol.* 53, 365–389. doi:10.1093/ptrology/egr065
- Rooney, T. O., Nelson, W. R., Dosso, L., Furman, T., Hanan, B., and Schilling, J.-G. (2014). The Role of continental Lithosphere Metasomes in the Production of HIMU-like Magmatism on the Northeast African and Arabian Plates. *Geology* 42, 419–422. doi:10.1130/G35216.1
- Rosenthal, A., Foley, S. F., Pearson, D. G., Nowell, G. M., and Tappe, S. (2009). Petrogenesis of Strongly Alkaline Primitive Volcanic Rocks at the Propagating Tip of the Western branch of the East African Rift. *Earth Planet. Sci. Lett.* 284, 236–248. doi:10.1016/j.epsl.2009.04.036
- Rudge, J. F., MacLennan, J., and Stracke, A. (2013). The Geochemical Consequences of Mixing Melts from a Heterogeneous Mantle. *Geochimica et Cosmochimica Acta* 114, 112–143. doi:10.1016/j.gca.2013.03.042
- Rukieh, M., Trifonov, V. G., Dodonov, A. E., Minini, H., Ammar, O., Ivanova, T. P., et al. (2005). Neotectonic Map of Syria and Some Aspects of Late Cenozoic Evolution of the Northwestern Boundary Zone of the Arabian Plate. *J. Geodynamics* 40, 235–256. doi:10.1016/j.jog.2005.07.016
- Sagnotti, L. (2013). Demagnetization Analysis in Excel (DAIE) - an Open Source Workbook in Excel for Viewing and Analyzing Demagnetization Data from Paleomagnetic Discrete Samples and U-Channels. *Ann. Geophys* 56, D0114. doi:10.4401/ag-6282
- Salters, V. J. M., and Dick, H. J. B. (2002). Mineralogy of the Mid-ocean-ridge basalt Source from Neodymium Isotopic Composition of Abyssal Peridotites. *Nature* 418, 68–72. doi:10.1038/nature00798
- Salters, V. J. M., and Stracke, A. (2004). Composition of the Depleted Mantle. *Geochem. Geophys. Geosyst.* 5, a–n. doi:10.1029/2003GC000597
- Sanfilippo, A., Cai, Y., Jácome, A. P. G., and Ligi, M. (2019). “Geochemistry of the Lunayyir and Khaybar Volcanic Fields (Saudi Arabia): Insights into the Origin of Cenozoic Arabian Volcanism,” in *Geological Setting, Palaeoenvironment and Archaeology of the Red Sea*. Editors N. M. A. Rasul and I. C. F. Stewart (Cham, Switzerland: Springer Earth System Science, Springer Nature), 389–415. doi:10.1007/978-3-319-99408-6_18
- Schilling, J.-G., Kingsley, R. H., Hanan, B. B., and McCully, B. L. (1992). Nd-Sr-Pb Isotopic Variations along the Gulf of Aden: Evidence for Afar Mantle Plume-Continental Lithosphere Interaction. *J. Geophys. Res.* 97, 10927–10966. doi:10.1029/92JB00415
- Schmidberger, S. S., Simonetti, A., Heaman, L. M., Creaser, R. A., and Whiteford, S. (2007). Lu-Hf, In-Situ Sr and Pb Isotope and Trace Element Systematics for Mantle Eclogites from the Diavik diamond Mine: Evidence for Paleoproterozoic Subduction beneath the Slave Craton, Canada. *Earth Planet. Sci. Lett.* 254, 55–68. doi:10.1016/j.epsl.2006.11.020
- Shaw, J. E., Baker, J. A., Kent, A. J. R., Ibrahim, K. M., and Menzies, M. A. (2007). The Geochemistry of the Arabian Lithospheric Mantle-Aa Source for Intraplate Volcanism?. *J. Petrol.* 48, 1495–1512. doi:10.1093/ptrology/egm027
- Shaw, J. E., Baker, J. A., Menzies, M. A., Thirlwall, M. F., and Ibrahim, K. M. (2003). Petrogenesis of the Largest Intraplate Volcanic Field on the Arabian Plate

- (Jordan): a Mixed Lithosphere-Asthenosphere Source Activated by Lithospheric Extension. *J. Petrol.* 44, 1657–1679. doi:10.1093/petrology/egg052
- Stein, M., and Goldstein, S. L. (1996). From Plume Head to continental Lithosphere in the Arabian-Nubian Shield. *Nature* 382, 773–778. doi:10.1038/382773a0
- Stein, M., and Hofmann, A. W. (1992). Fossil Plume Head beneath the Arabian Lithosphere?. *Earth Planet. Sci. Lett.* 114, 193–209. doi:10.1016/0012-821X(92)90161-N
- Stein, M., Navon, O., and Kessel, R. (1997). Chromatographic Metasomatism of the Arabian-Nubian Lithosphere. *Earth Planet. Sci. Lett.* 152, 75–91. doi:10.1016/S0012-821X(97)00156-8
- Stern, R. J., and Johnson, P. (2010). Continental Lithosphere of the Arabian Plate: a Geologic, Petrologic, and Geophysical Synthesis. *Earth-Science Rev.* 101, 29–67. doi:10.1016/j.earscirev.2010.01.002
- Stewart, K., and Rogers, N. (1996). Mantle Plume and Lithosphere Contributions to Basalts from Southern Ethiopia. *Earth Planet. Sci. Lett.* 139, 195–211. doi:10.1016/0012-821X(96)00015-5
- Stracke, A., Bizimis, M., and Salters, V. J. M. (2003). Recycling Oceanic Crust: Quantitative Constraints. *Geochem. Geophys. Geosyst.* 4, 8003. doi:10.1029/2001GC000223
- Stracke, A. (2012). Earth's Heterogeneous Mantle: A Product of Convection-Driven Interaction between Crust and Mantle. *Chem. Geology.* 330–331, 274–299. doi:10.1016/j.chemgeo.2012.08.007
- Stracke, A., Genske, F., Berndt, J., and Koornneef, J. M. (2019). Ubiquitous Ultra-depleted Domains in Earth's Mantle. *Nat. Geosci.* 12, 851–855. doi:10.1038/s41561-019-0446-z
- Stracke, A. (2016). “Mantle Geochemistry,” in *Encyclopedia of Geochemistry. Encyclopedia of Earth Sciences Series*. Editor W. White (Cham: Springer), 1–12. doi:10.1007/978-3-319-39193-9_286-2
- Sun, S.-s., and McDonough, W. F. (1989). “Chemical and Isotopic Systematics of Oceanic Basalts: Implications for Mantle Composition and Processes,”. *Magmatism in Ocean Basins*. Editors A. D. Saunders and M. J. Norry (London: Geol. Soc. London, Special Publication), 42, 313–345. doi:10.1144/GSL.SP.1989.042.01.19
- Tackley, P. J. (2015). “Mantle Geochemical Geodynamics,”. *Treatise on Geophysics*. Editors D. Bercovici and G. Schubert. Second Edition (Elsevier), 7, 521–585. doi:10.1016/B978-0-444-53802-4.00134-2
- Tanaka, T., Togashi, S., Kamioka, H., Amakawa, H., Kagami, H., Hamamoto, T., et al. (2000). JNd-1: a Neodymium Isotopic Reference in Consistency with Lajolla Neodymium. *Chem. Geology.* 168, 279–281. doi:10.1016/S0009-2541(00)00198-4
- Thybo, H., and Nielsen, C. A. (2009). Magma-compensated Crustal Thinning in continental Rift Zones. *Nature* 457, 873–876. doi:10.1038/nature07688
- Tilton, G. R., and Bell, K. (1994). Sr-Nd-Pb Isotope Relationships in Late Archean Carbonatites and Alkaline Complexes: Applications to the Geochemical Evolution of Archean Mantle. *Geochimica et Cosmochimica Acta* 58, 3145–3154. doi:10.1016/0016-7037(94)90042-6
- Todt, W., Cliff, R. A., Hanser, A., and Hofmann, A. W. (1996). “Evaluation of a ²⁰²Pb-²⁰⁵Pb Double Spike for High Precision lead Isotopic Analysis,”. *Earth Processes: Reading the Isotopic Code*. Editors A. Basu and S. Hart (Washington DC: American Geophysical Union/Geophysical Monograph), 95, 429–437.
- Tormey, D. R., Grove, T. L., and Bryan, W. B. (1987). Experimental Petrology of normal MORB Near the Kane Fracture Zone: 22° 25' N, Mid-Atlantic ridge. *Contr. Mineral. Petrol.* 96, 121–139. doi:10.1007/BF00375227
- Unterschutz, J. L. E., Creaser, R. A., Erdmer, P., Thompson, R. I., and Daughy, K. L. (2002). North American Margin Origin of Quesnel Terrane Strata in the Southern Canadian Cordillera: Inferences from Geochemical and Nd Isotopic Characteristics of Triassic Metasedimentary Rocks. *Geol. Soc. Am. Bull.* 114, 462–475. doi:10.1130/0016-7606(2002)114<0462:NAMOOQ>2.0.CO;2
- Vaslet, D., Janjou, D., Robelin, C., Al-Muallem, M. S., Halawani, M. A., Brosse, J.-M., et al. (1994). Geologic Map of the Tayma Quadrangle, Sheet 27C, Kingdom of Saudi Arabia. scale 1:250,000, with explanatory text. Jeddah: Saudi Arabian Directorate General of Mineral Resources Geoscience Map GM-134, 51.
- Vidal, P., Deniel, C., Vellutini, P. J., Piguet, P., Coulon, C., Vincent, J., et al. (1991). Changes of Mantle Sources in the Course of a Rift Evolution: The Afar Case. *Geophys. Res. Lett.* 18, 1913–1916. doi:10.1029/91GL02006
- Vigliotti, L., Cai, Y., Rasul, N. M. A., and Al-Nomani, S. M. S. (2019). “Palaeomagnetism and Geochronology of the Harrats Lunayyir and Khaybar Lava Fields, Saudi Arabia,” in *Geological Setting, Palaeoenvironment and Archaeology of the Red Sea*. Editors N. M. A. Rasul and I. C. F. Stewart (Cham, Switzerland: Springer Earth System Science, Springer Nature), 417–435. doi:10.1007/978-3-319-99408-6_19
- Volker, F., Altherr, R., Jochum, K.-P., and McCulloch, M. T. (1997). Quaternary Volcanic Activity of the Southern Red Sea: New Data and Assessment of Models on Magma Sources and Afar Plume-Lithosphere Interaction. *Tectonophysics* 278, 15–29. doi:10.1016/S0040-1951(97)00092-9
- Volker, F., McCulloch, M. T., and Altherr, R. (1993). Submarine Basalts from the Red Sea: New Pb, Sr, and Nd Isotopic Data. *Geophys. Res. Lett.* 20, 927–930. doi:10.1029/93GL00050
- Weinstein, Y., Navon, O., Altherr, R., and Stein, M. (2006). The Role of Lithospheric Mantle Heterogeneity in the Generation of Plio-Pleistocene Alkali Basaltic Suites from NW Harrat Ash Shaam (Israel). *J. Petrol.* 47, 1017–1050. doi:10.1093/petrology/egl100310.1093/petrology/egl1003
- Weiss, Y., Class, C., Goldstein, S. L., and Hanyu, T. (2016). Key New Pieces of the HIMU Puzzle from Olivines and diamond Inclusions. *Nature* 537, 666–670. doi:10.1038/nature19113
- White, R. S., Smith, L., Smith, L. K., Roberts, A. W., Christie, P. A. F., and Kusznir, N. J. (2008). Lower-crustal Intrusion on the North Atlantic continental Margin. *Nature* 452, 460–464. doi:10.1038/nature06687
- Yang, H.-J., Kinzler, R. J., and Grove, T. L. (1996). Experiments and Models of Anhydrous, Basaltic Olivine-Plagioclase-Augite Saturated Melts from 0.001 to 10 Kbar. *Contrib. Mineralogy Petrol.* 124, 1–18. doi:10.1007/s004100050169
- Zahrn, H. M., Stewart, I. C. F., Johnson, P. R., and Basahel, M. H. (2003). “Aeromagnetic-anomaly Maps of central and Western Saudi Arabia. Scale 1:2 Million,”. Open-File Report SGS-OF-2002-8 (Jeddah: Saudi Geological Survey), 6.
- Zimmer, M., Kröner, A., Jochum, K. P., Reischmann, T., and Todt, W. (1995). The Gabal Gerf Complex: A Precambrian N-MORB Ophiolite in the Nubian Shield, NE Africa. *Chem. Geology.* 123, 29–51. doi:10.1016/0009-2541(95)00018-H
- Zindler, A., and Hart, S. (1986). Chemical Geodynamics. *Annu. Rev. Earth Planet. Sci.* 14, 493–571. doi:10.1146/annurev.ea.14.050186.002425

Conflict of Interest: Author IS was employed by the company Stewart Geophysical Consultants Pty. Ltd.

The remaining authors declare that the research was conducted in the absence of any commercial or financial relationships that could be construed as a potential conflict of interest.

Publisher's Note: All claims expressed in this article are solely those of the authors and do not necessarily represent those of their affiliated organizations, or those of the publisher, the editors and the reviewers. Any product that may be evaluated in this article, or claim that may be made by its manufacturer, is not guaranteed or endorsed by the publisher.

Copyright © 2021 Sanfilippo, Sani, Rasul, Stewart, Vigliotti, Widinly, Osemi and Ligi. This is an open-access article distributed under the terms of the Creative Commons Attribution License (CC BY). The use, distribution or reproduction in other forums is permitted, provided the original author(s) and the copyright owner(s) are credited and that the original publication in this journal is cited, in accordance with accepted academic practice. No use, distribution or reproduction is permitted which does not comply with these terms.